

# *ANN-based Model of Continuous Casting of Steel*

## *Detailed Study*

Igor Grešovnik  
Tadej Kodelja

*Centre of Excellence for Biosensors, Instrumentation and Process Control*

*Revision 7, September 2013.*  
(revision 0: Nov. 2012)

**Warning:** This is a long document; **please don't send it to a printer!**





## Contents:

<b>1</b>	<b><i>Introduction</i></b> .....	<b>1</b>
<b>2</b>	<b><i>Process Parameters and Final Material Properties</i></b> .....	<b>2</b>
<b>3</b>	<b><i>ANN Modeling Software</i></b> .....	<b>4</b>
<b>4</b>	<b><i>Convergence</i></b> .....	<b>6</b>
<b>4.1</b>	<b>Search for Best ANN Settings (1000 TP)</b> .....	<b>6</b>
4.1.1	Maximum Errors on Training Points .....	6
4.1.2	Rms Errors on Training Points.....	8
4.1.3	Maximum Errors on Verification Points.....	10
4.1.4	Rms Errors on Verification Points .....	12
<b>4.2</b>	<b>Search for Best ANN Architecture (1000 TP)</b> .....	<b>13</b>
4.2.1	Maximum Errors on Training Points .....	14
4.2.2	Rms Errors on Training Points.....	15
4.2.3	Maximum Errors on Verification Points.....	17
4.2.4	Rms Errors on Verification Points .....	19
<b>4.3</b>	<b>Search for Best ANN Architecture for Different Training Data-sets</b> .....	<b>21</b>
4.3.1	Training on 100 Training Sets .....	21
4.3.2	Training on 200 Training Sets .....	23
4.3.3	Training on 500 Training Sets .....	25
4.3.4	Training on 1000 Training Sets .....	28
4.3.5	Training on 2000 Training Sets .....	30
4.3.6	Training on 5000 Training Sets .....	32
4.3.7	Training on 10000 Training Sets .....	35
4.3.8	Best Architecture for Different Training Sets .....	37
<b>5</b>	<b><i>Error Estimation</i></b> .....	<b>39</b>
<b>5.1</b>	<b>Maximum Errors on Different Training Sets</b> .....	<b>39</b>
<b>6</b>	<b><i>Training ANN on Optimal Training Sets</i></b> .....	<b>40</b>
<b>6.1</b>	<b>Error Estimation</b> .....	<b>40</b>
6.1.1	Metallurgical Length (ML) .....	40
6.1.2	Shell Thickness at the end of the Mould (DS) .....	41
6.1.3	Billet Surface Temperature at Straightening Start Position (T) .....	42
<b>6.2</b>	<b>Parametric studies</b> .....	<b>44</b>
6.2.1	Center Point .....	44
6.2.2	Points on Line .....	54
<b>6.3</b>	<b>Sensitivity Tests</b> .....	<b>62</b>
6.3.1	Metallurgical Length (ML) .....	62
6.3.2	Shell Thickness at the End of the Mould (DS) .....	63
6.3.3	Billet Surface Temperature at Straightening Start Position (T) .....	64

## 1 INTRODUCTION

This report provides detailed description of results of the artificial neural network-based modeling of the continuous casting process in the Štore Steel [1] company. This is currently the only part of the process for which the company has access to numerical simulator, and therefore the only part of the process for which a reliable ANN model can be constructed.

The model was constructed on basis of the Robert Vertnik's casting simulator [2]-[4], which was used to produce training data. Construction and analysis of the model was performed by the *NeuralShell*, a flexible multilayered interpreter-centered ANN modeling software *Investigative Generic Library (IGLib)*. Concepts used in this software have evolved in several years of research work on optimization, inverse analysis and approximation models, which finally culminated in the *IGLib* [5]-[13] library that is used as code base for demanding technical applications. The code depicts on several third party libraries used for the solution of different tasks, which are mentioned in the IGLib web page. Among these, the Aforge.Net [14] library is used as the library for neural networks-related tasks.

The process modeled is briefly described in Section 2. Section 3 contains a short description of the software that was used for generation and analysis of the model. In Section 4 we describe the search for the best ANN model for this example. In the scope of this, we have tested several combinations of ANN architectures and training parameters, which was done by using the IGLib's generic training modules. Section 5 is dedicated to validation of the results and estimation of errors. Section 6 contains a detailed depiction of results of the developed ANN model. This part is the most interesting for practical use and for industrial people involved in the modeled process.

## **2 PROCESS PARAMETERS AND FINAL MATERIAL PROPERTIES**

**Process parameters are shown in**

Table 1 and output values are shown in Table 2 for the current example.

**Table 1:** Process parameters (input parameters).

VALUES	NUMBER
Casting temperature (Tcast)	1
Casting speed (v)	1
Temperature difference of cooling water in the mould (DTmould)	1
Cooling flow rate in the mould (Qmould)	1
Cooling flow rate in wreath spray system (Qwreath)	1
Cooling flow rate in 1st spray system (Qsistem1)	1
<b>TOTAL</b>	<b>6</b>

**Table 2:** Output values.

VALUES	NUMBER
Metallurgical length (ML)	1
Shell thickness at the end of the mould (DS)	1
Billet surface temperature at straightening start position (T)	1
<b>TOTAL</b>	<b>3</b>

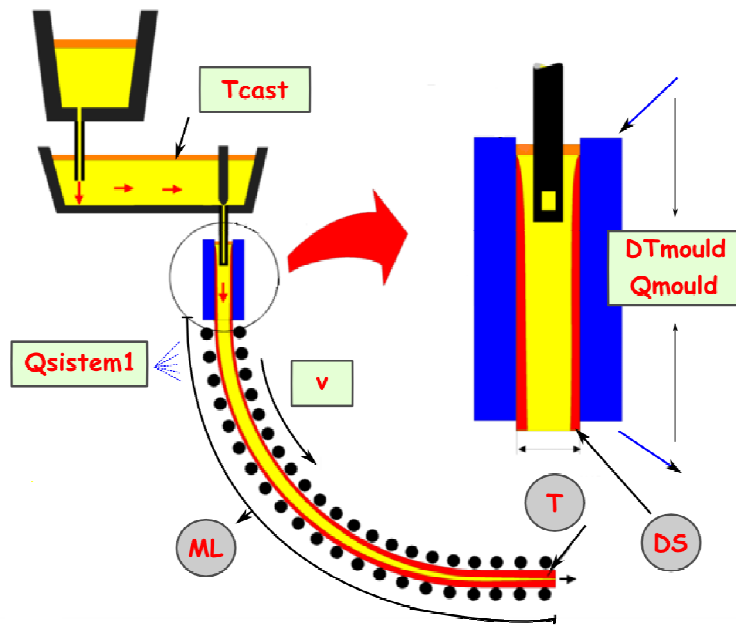


**Figure 1:** Location of process parameters and output values in the continuous casting process.

### 3 ANN MODELING SOFTWARE

A software for construction and use of ANN-based models has been developed in the scope of this work. The software was designed as to match the challenges and requirements met when solving this kind of problems. In particular, it must provide good flexibility in designing training strategies, filtering training data, verification of results, testing different network layouts, integration with other software, etc. This is crucial when approximating behavior of steel processing systems with large number of processing parameters. Data obtained from such systems is often inaccurate or even corrupted due to practical limitations in acquisition procedures. Response sampling can not be planned in advance but is accommodated to production schedules in the factory, therefore information available may be deficient in some regions of parameter space in order to obtain good response approximation and therefore verification of results plays an important role.

The software is based on *IGLib* [13], a specialized framework for efficient development of demanding technical applications, and inherits the majority of design paradigms from this framework. Some of these concepts historically follow from the experience gained in development of general purpose optimization software [8]-[12], which is subjected to similar requirements regarding the modularity of software and sufficient flexibility of its user interfaces to accommodate to dynamic environment of multidisciplinary research and development. Among the others, this historical concept is the origin of postulation that a suitable interface for defining and solving complex optimization problems should include a full interpreter capability, through which the built-in functionality, packed in modular libraries, is accessed. Two-level interpreter system developed in IGLib on basis of this experience is utilized in our software and enables rapid reactions to changing demands as new knowledge is gained from the results. IGLib also incorporates design of approximation-based modeling utilities emerging from the development of optimization libraries [10]-[12]. In the scope of the framework, the elaborate object oriented design was supplemented by a number of advanced concepts directed towards rapid application development. These include adherence the concepts of .NET frameworks and extensive use of generic programming. Yet another design feature brought by IGLib is typical arrangement of the framework libraries in a number of levels according to criteria such as platform dependency or license restrictions. The software relies on a number of third party libraries that are mainly distributed under permissive open source licenses.

The Aforge.Net library is used as ANN framework [14]. A convenient characteristics of neural networks is that approximation can be performed in two separate stages (Figure 2). In the training stage, the network is trained by using the sampled response (either measured or calculated by a numerical model). In the approximation stage, trained network is used for all subsequent calculations of approximated response at arbitrary values of input parameters. This gives neural networks an important advantage over other modeling techniques, since the second stage is very fast as compared to the first stage. The software takes full advantage of this feature by separating these stages. This is especially important when performing extensive analyses of the considered process on basis of the developed ANN models, or when incorporating the models in automatic optimization procedures [16],[17].

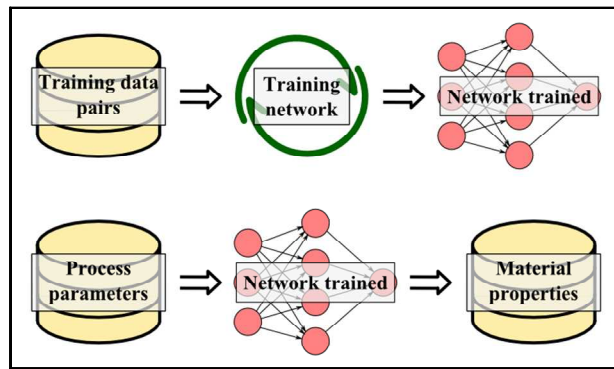


**Figure 2:** Approximation with neural networks: training a network with presented data pairs (top) and calculation of approximated response with trained network (bottom).

## 4 CONVERGENCE

### 4.1 Search for Best ANN Settings (1000 TP)

**Table 3:** Best ANN settings.

Name	Value
Number of hidden layers	1
Number of neurons in hidden layer 1	25
Maximum number of epochs	150.000
Learning rate	0.6
Momentum	0.5
Input safety factor	1.4
Output safety factor	1.4

#### 4.1.1 Maximum Errors on Training Points

##### 4.1.1.1 Metallurgical length (ML)

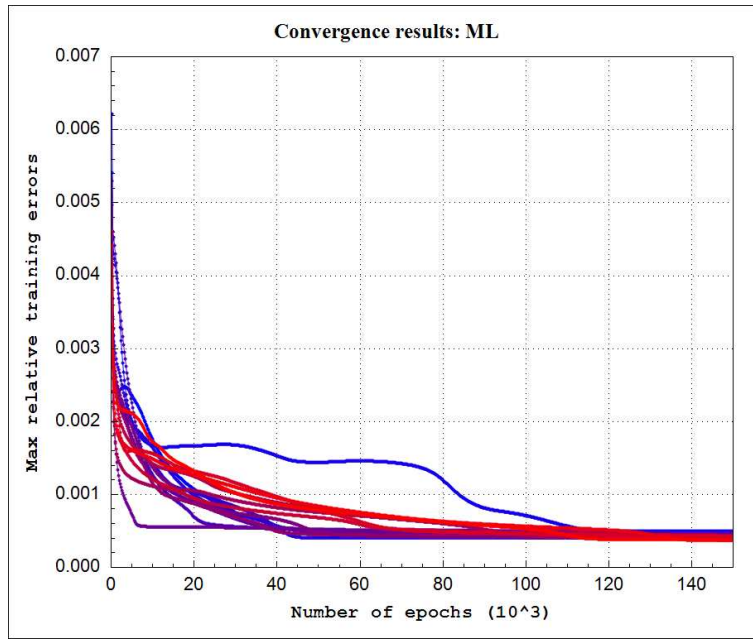


**Figure 3:** Convergence of maximum errors on training points for metallurgical length (ML).

#### 4.1.1.2 Shell Thickness at the End of the Mould (DS)

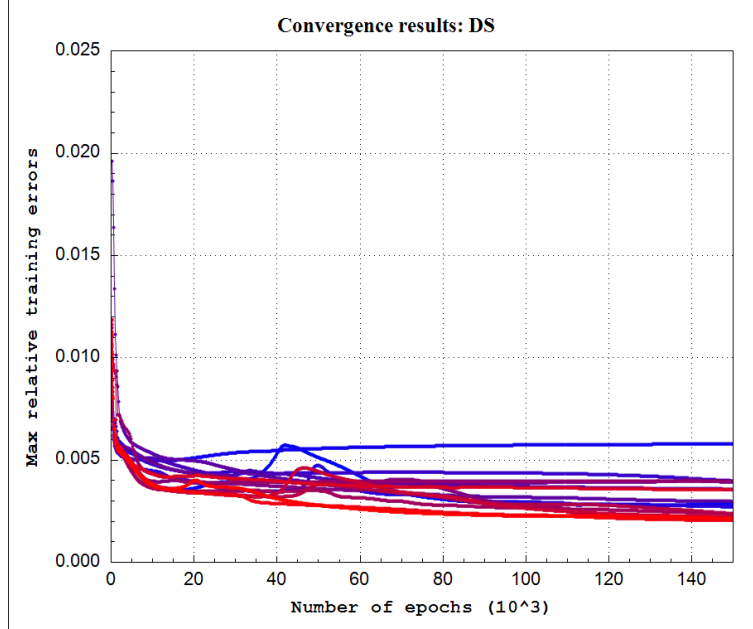


**Figure 4:** Convergence of maximum errors on training points for shell thickness at the end of the mould (DS).

#### 4.1.1.3 Billet Surface Temperature at Straightening Start Position (T)

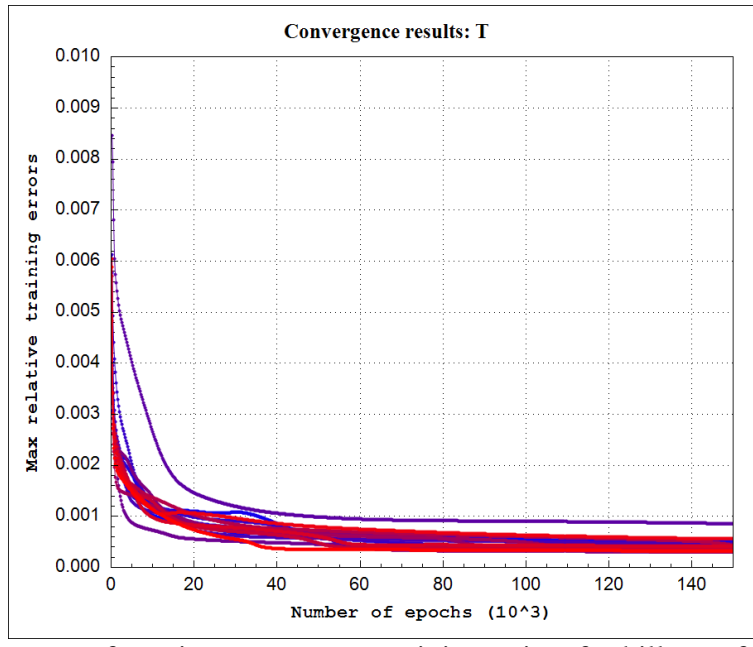


**Figure 5:** Convergence of maximum errors on training points for billet surface temperature at straightening start position (T).

#### 4.1.2 Rms Errors on Training Points

##### 4.1.2.1 Metallurgical length (ML)

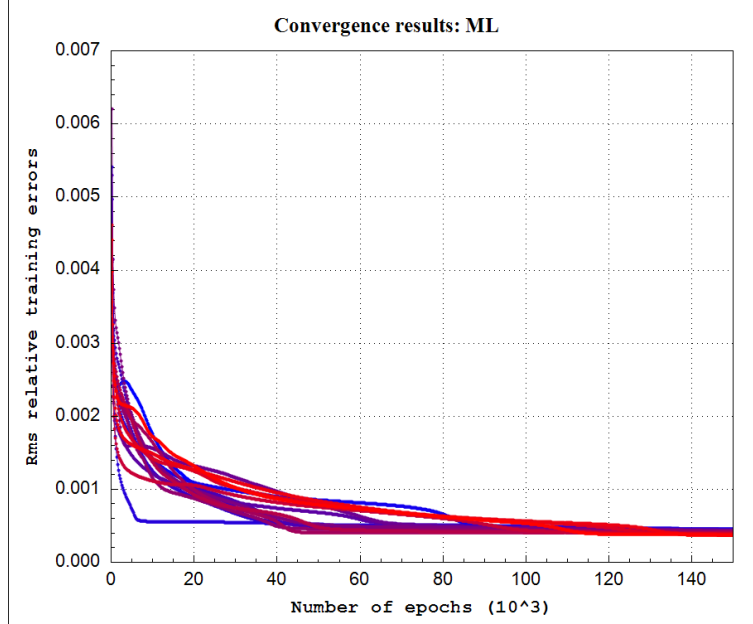


**Figure 6:** Convergence of Rms errors on training points for metallurgical length (ML).

#### 4.1.2.2 Shell Thickness at the End of the Mould (DS)

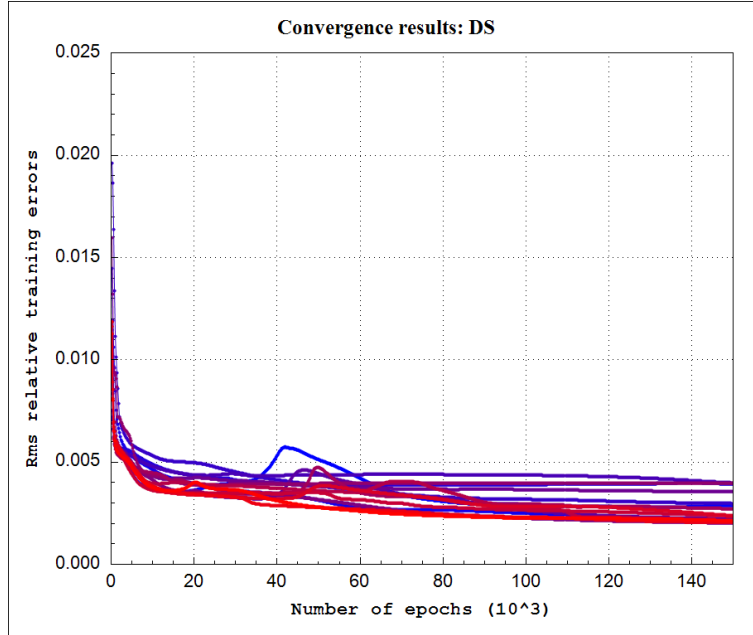


**Figure 7:** Convergence of Rms errors on training points for shell thickness at the end of the mould (DS).

#### 4.1.2.3 Billet Surface Temperature at Straightening Start Position (T)

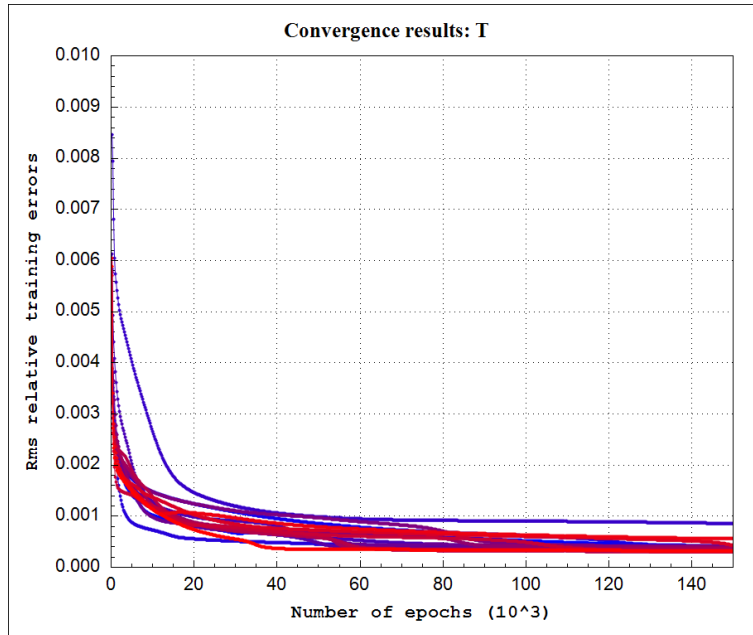


**Figure 8:** Convergence of Rms errors on training points for billet surface temperature at straightening start position (T).

#### 4.1.3 Maximum Errors on Verification Points

##### 4.1.3.1 Metallurgical length (ML)

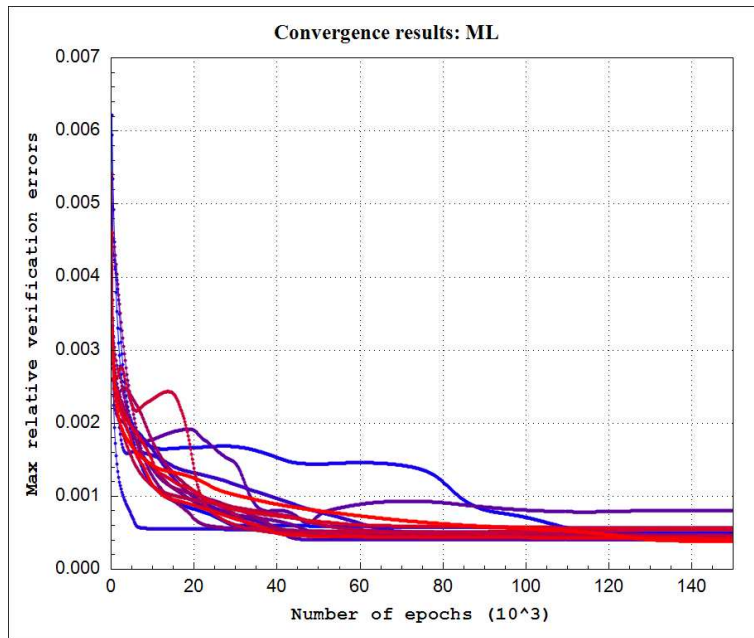


**Figure 9:** Convergence of maximum errors on verification points for metallurgical length (ML).

##### 4.1.3.2 Shell Thickness at the End of the Mould (DS)

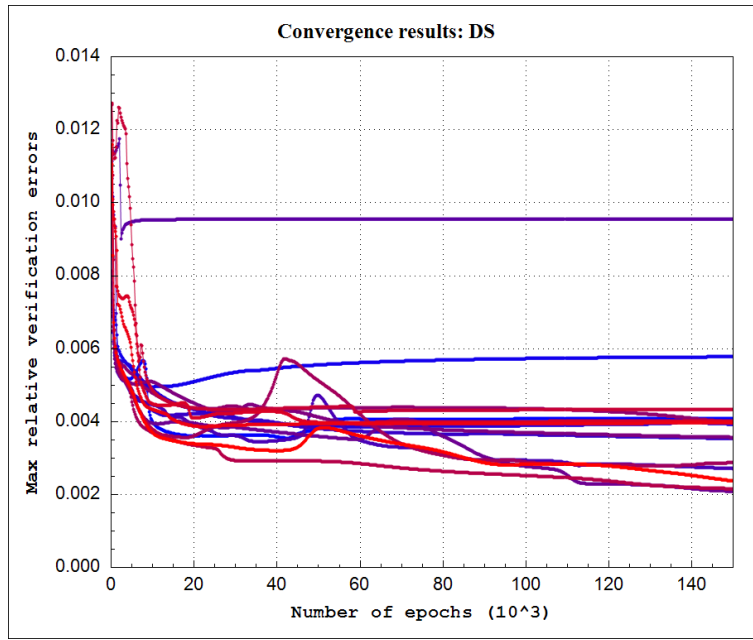


**Figure 10:** Convergence of maximum errors on verification points for shell thickness at the end of the mould (DS).

#### 4.1.3.3 Billet Surface Temperature at Straightening Start Position (T)

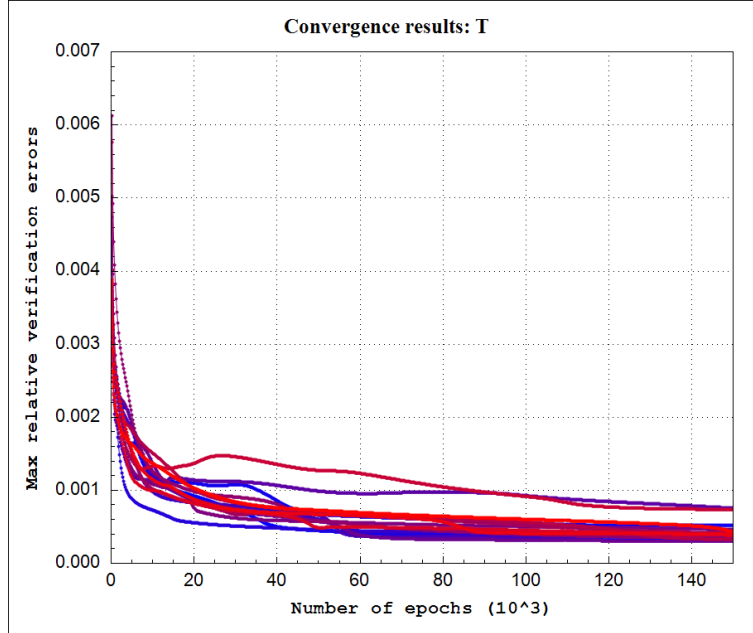


**Figure 11:** Convergence of maximum errors on verification points for billet surface temperature at straightening start position (T).

#### 4.1.4 Rms Errors on Verification Points

##### 4.1.4.1 Metallurgical length (ML)

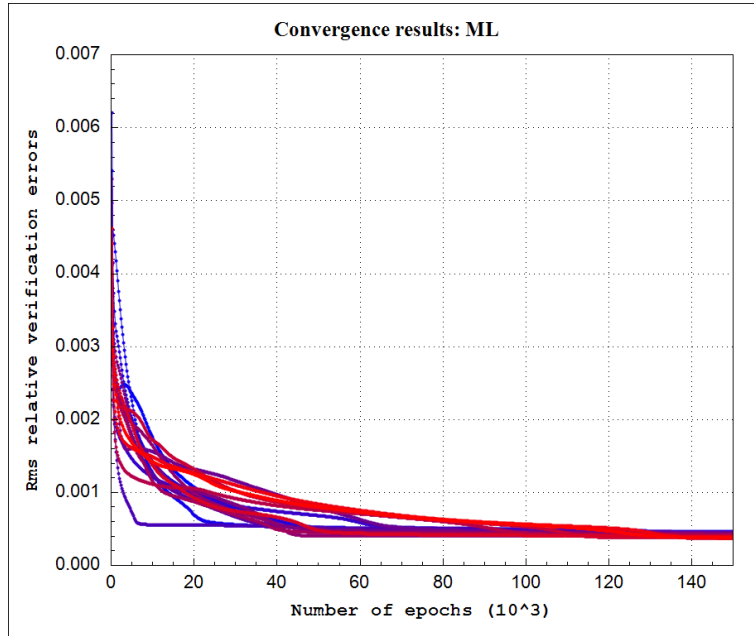
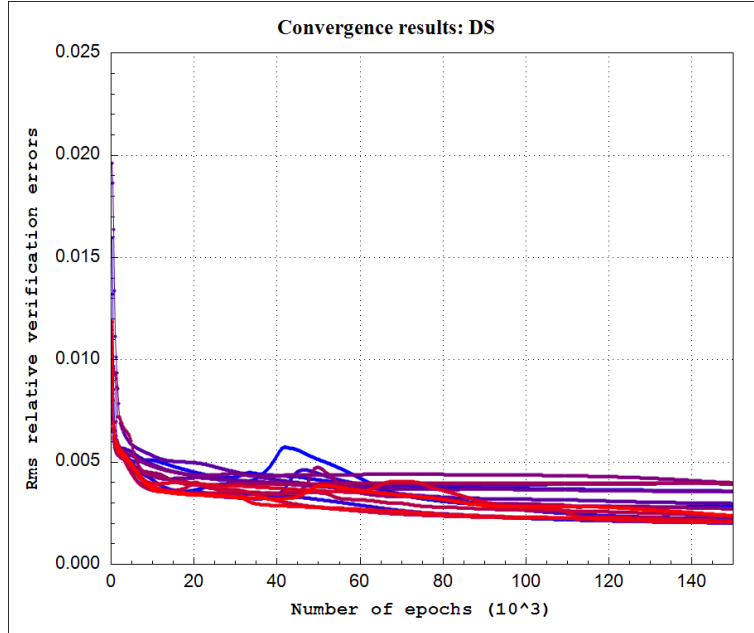


Figure 12: Convergence of Rms errors on verification points for metallurgical length (ML).

##### 4.1.4.2 Shell Thickness at the End of the Mould (DS)



**Figure 13:** Convergence of Rms errors on verification points for shell thickness at the end of the mould (DS).

#### 4.1.4.3 Billet Surface Temperature at Straightening Start Position (T)

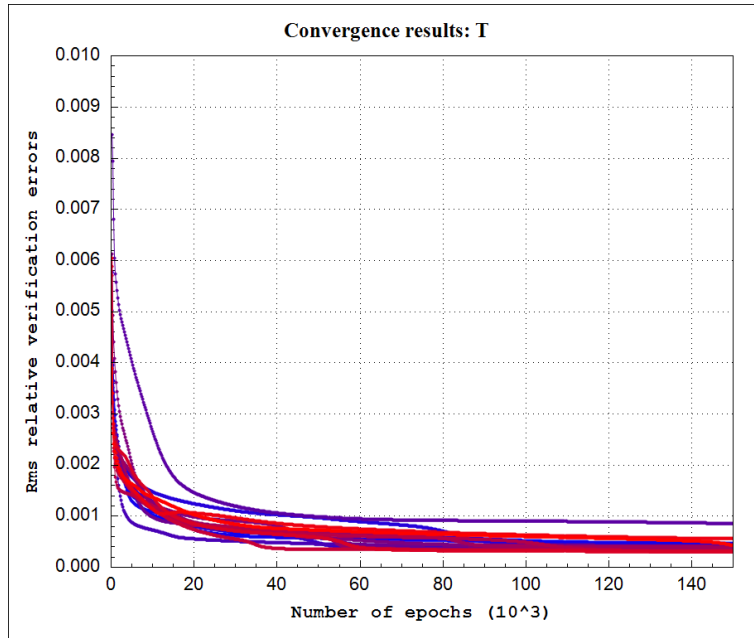


**Figure 14:** Convergence of Rms errors on verification points for billet surface temperature at straightening start position (T).

## 4.2 Search for Best ANN Architecture (1000 TP)

**Table 4:** Best ANN architecture.

Name	Value
Number of hidden layers	2
Number of neurons in hidden layer 1	16
Number of neurons in hidden layer 2	20
Maximum number of epochs	150.000
Learning rate	0.6
Momentum	0.5
Input safety factor	1.4
Output safety factor	1.4

### 4.2.1 Maximum Errors on Training Points

#### 4.2.1.1 Metallurgical length (ML)

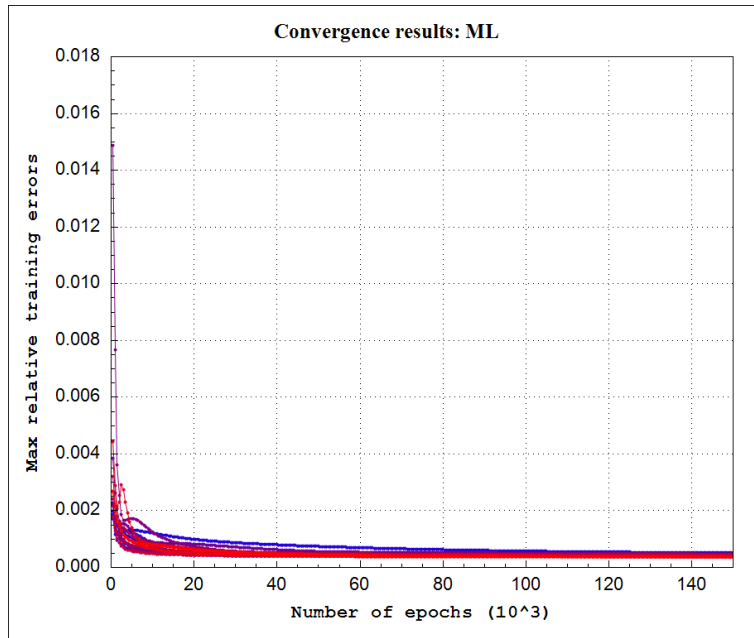
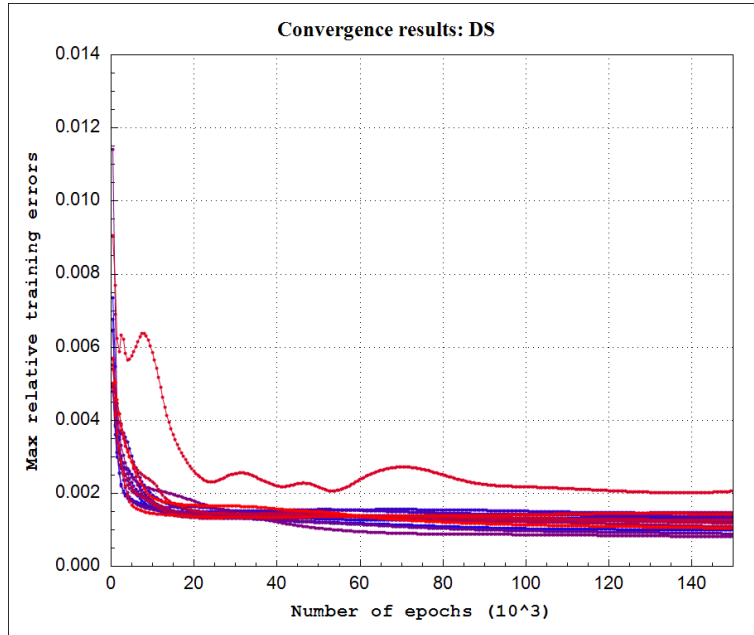


Figure 15: Convergence of maximum errors on training points for metallurgical length (ML).

#### 4.2.1.2 Shell Thickness at the End of the Mould (DS)



**Figure 16:** Convergence of maximum errors on training points for shell thickness at the end of the mould (DS).

#### 4.2.1.3 Billet Surface Temperature at Straightening Start Position (T)

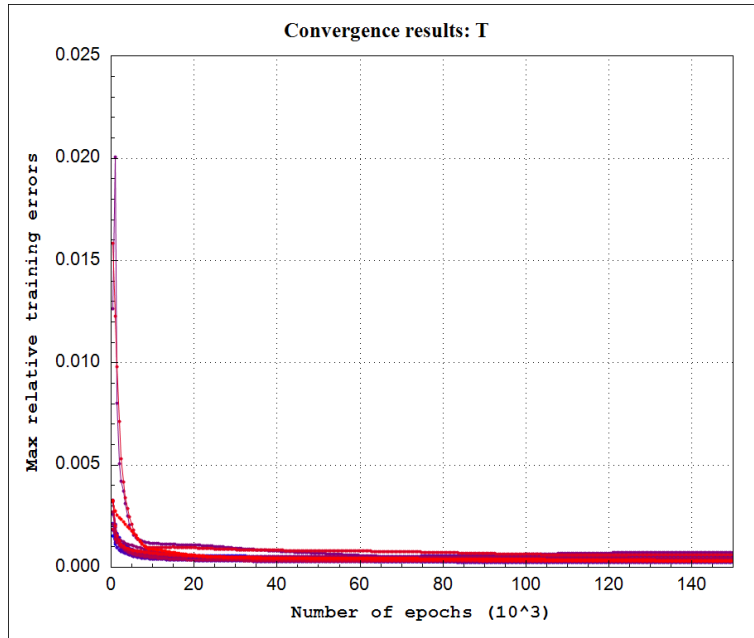


**Figure 17:** Convergence of maximum errors on training points for billet surface temperature at straightening start position (T).

#### 4.2.2 Rms Errors on Training Points

##### 4.2.2.1 Metallurgical length (ML)

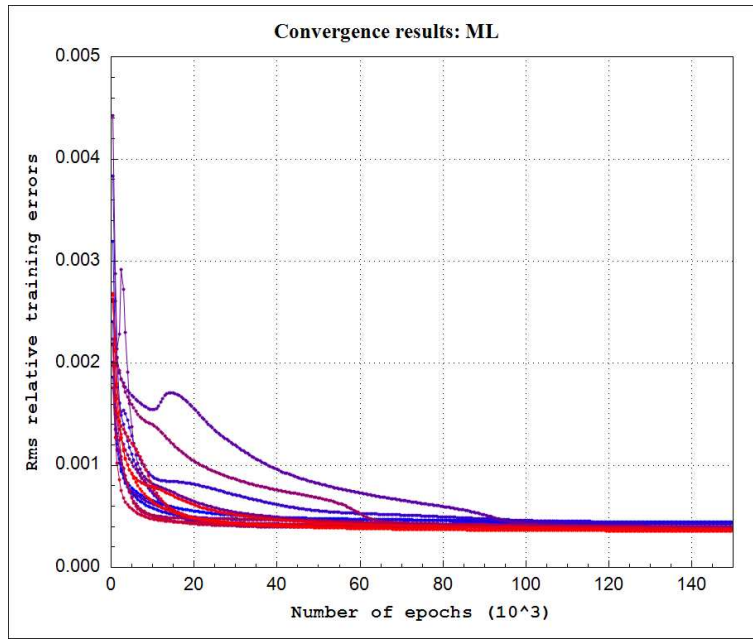


**Figure 18:** Convergence of Rms errors on training points for metallurgical length (ML).

#### 4.2.2.2 Shell Thickness at the End of the Mould (DS)

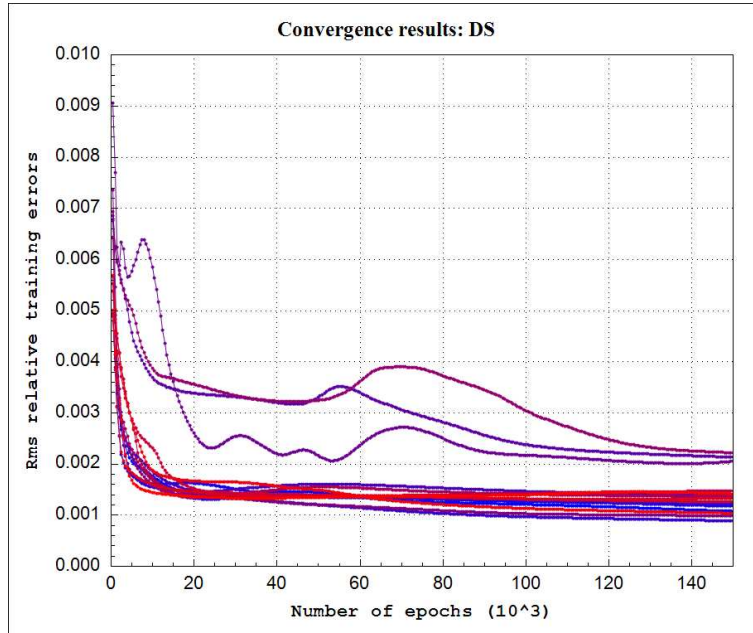


**Figure 19:** Convergence of Rms errors on training points for shell thickness at the end of the mould (DS).

#### 4.2.2.3 Billet Surface Temperature at Straightening Start Position (T)

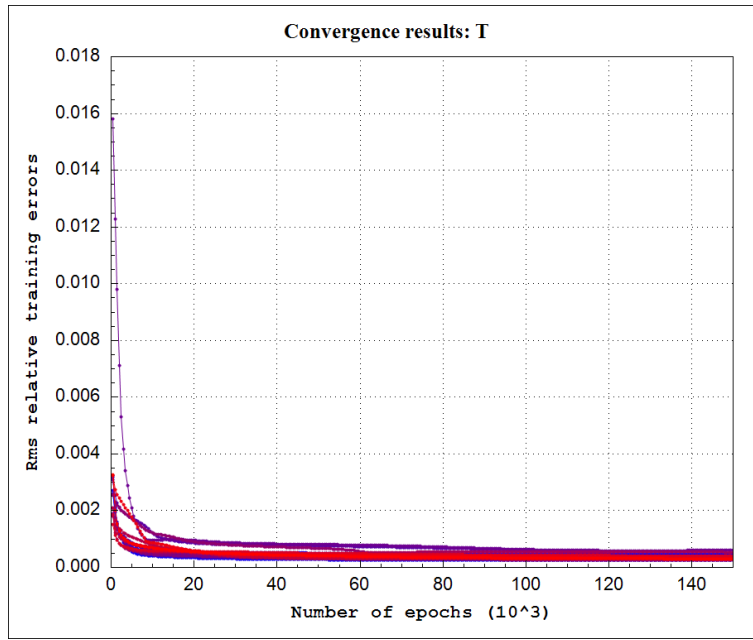


**Figure 20:** Convergence of Rms errors on training points for billet surface temperature at straightening start position (T).

#### 4.2.3 Maximum Errors on Verification Points

##### 4.2.3.1 Metallurgical length (ML)

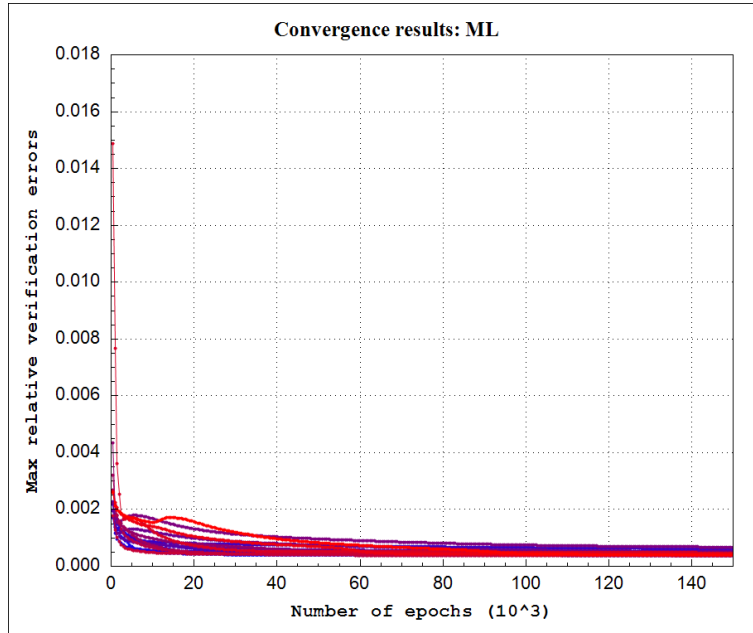


**Figure 21:** Convergence of maximum errors on verification points for metallurgical length (ML).

#### 4.2.3.2 Shell Thickness at the End of the Mould (DS)

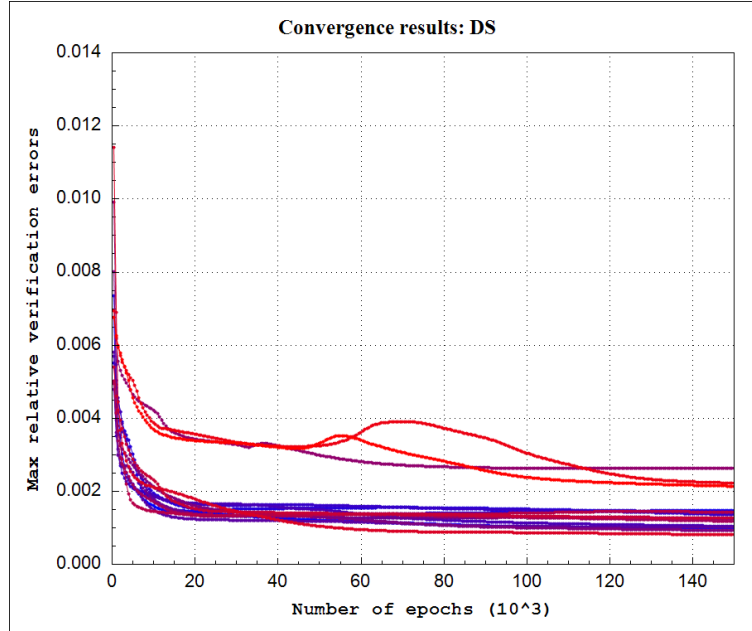


**Figure 22:** Convergence of maximum errors on verification points for shell thickness at the end of the mould (DS).

#### 4.2.3.3 Billet Surface Temperature at Straightening Start Position (T)

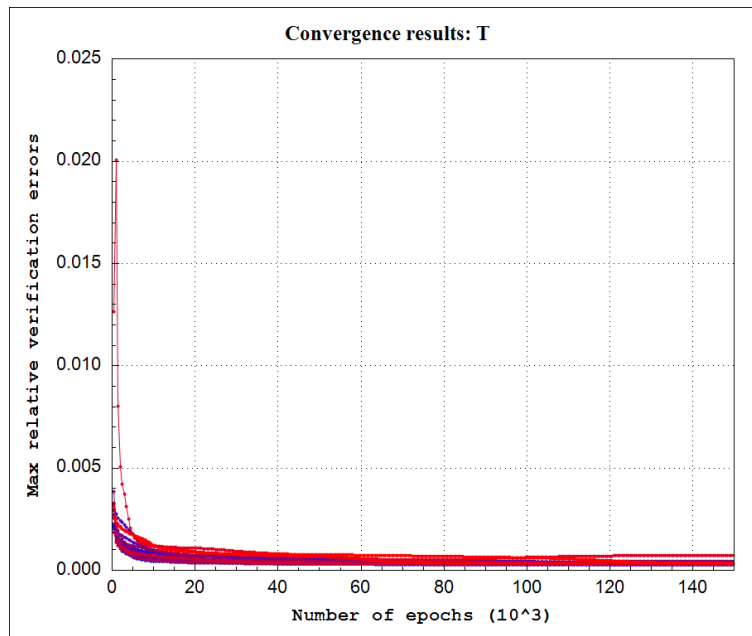


**Figure 23:** Convergence of maximum errors on verification points for billet surface temperature at straightening start position (T).

#### 4.2.4 Rms Errors on Verification Points

##### 4.2.4.1 Metallurgical length (ML)

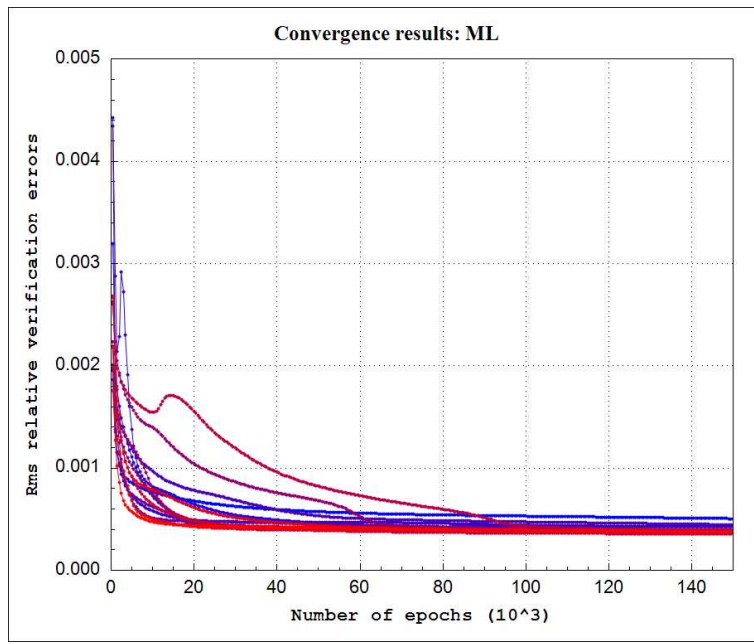


**Figure 24:** Convergence of Rms errors on verification points for metallurgical length (ML).

##### 4.2.4.2 Shell Thickness at the End of the Mould (DS)

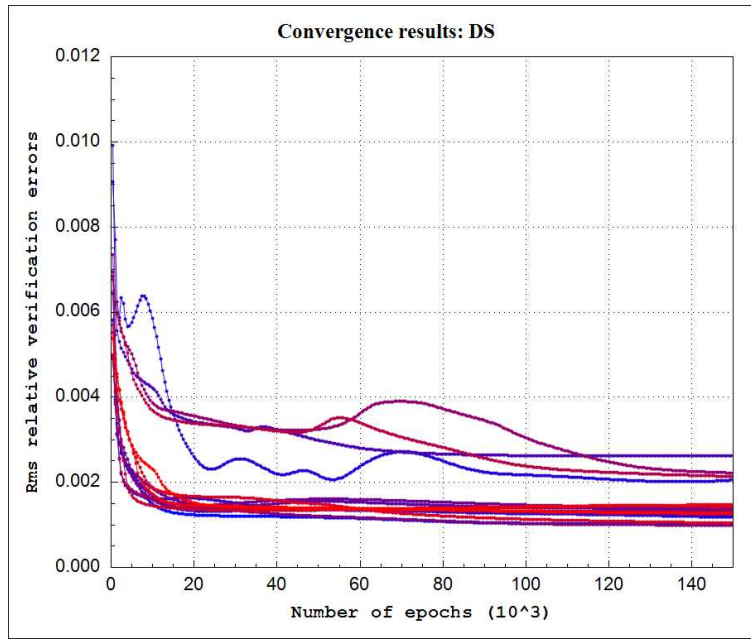


**Figure 25:** Convergence of Rms errors on verification points for shell thickness at the end of the mould (DS).

#### 4.2.4.3 Billet Surface Temperature at Straightening Start Position (T)

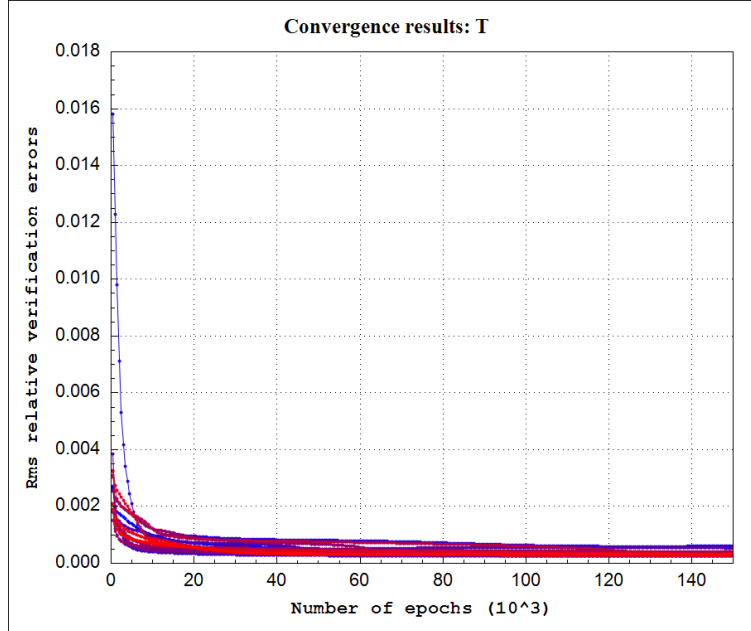


**Figure 26:** Convergence of Rms errors on verification points for billet surface temperature at straightening start position (T).

### 4.3 Search for Best ANN Architecture for Different Training Data-sets

#### 4.3.1 Training on 100 Training Sets

##### 4.3.1.1 Metallurgical length (ML)

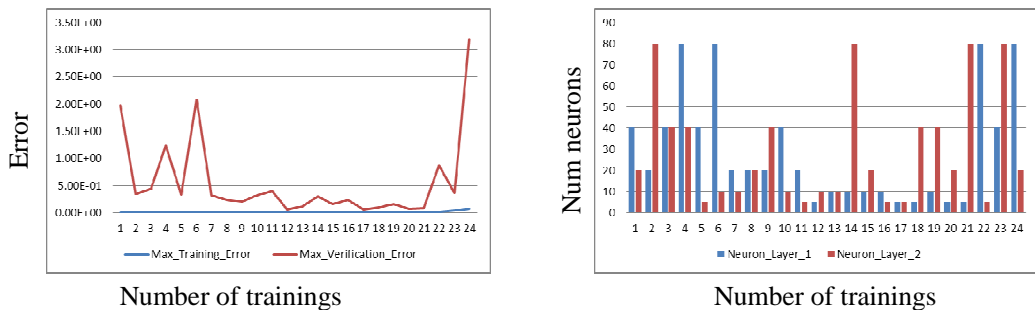


**Figure 27:** Maximum training errors and maximum verification errors on different architecture settings for metallurgical length (ML), trained on 100 training sets.

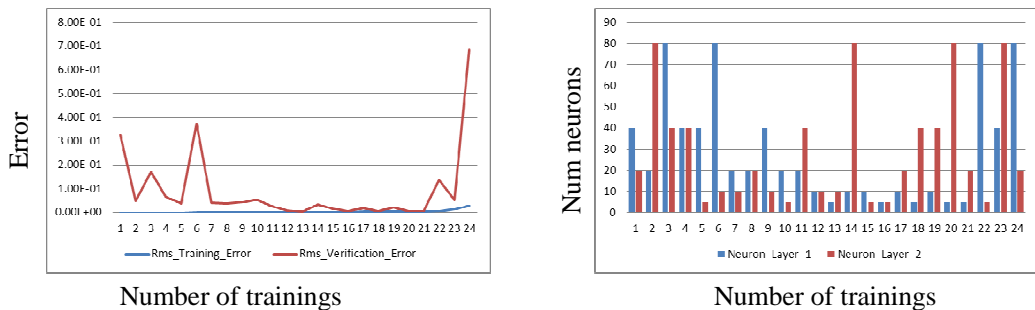


**Figure 28:** Rms training errors and Rms verification errors on different architecture settings for metallurgical length (ML), trained on 100 training sets.

##### 4.3.1.2 Shell Thickness at the End of the Mould (DS)

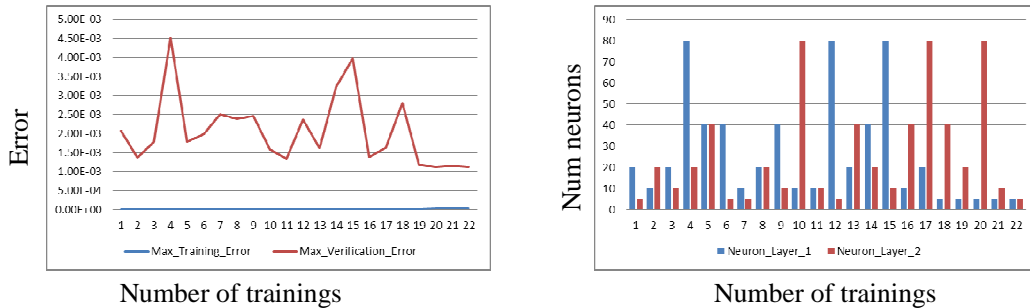


**Figure 29:** Maximum training errors and maximum verification errors on different architecture settings for shell thickness at the end of the mould (DS), trained on 100 training sets.

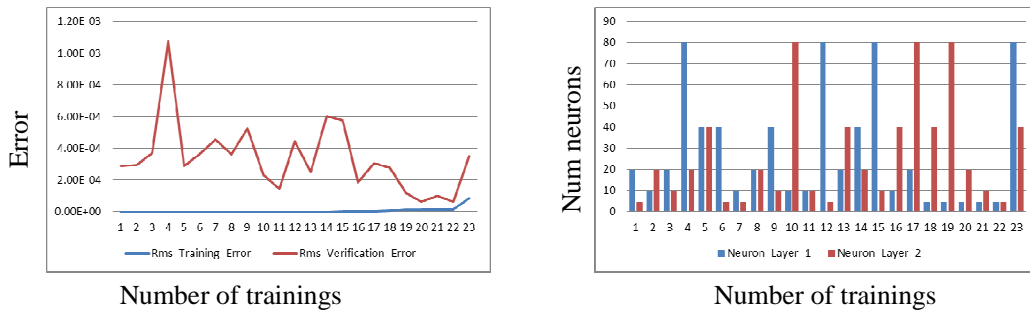


**Figure 30:** Rms training errors and Rms verification errors on different architecture settings for shell thickness at the end of the mould (DS), trained on 100 training sets.

#### 4.3.1.3 Billet Surface Temperature at Straightening Start Position (T)

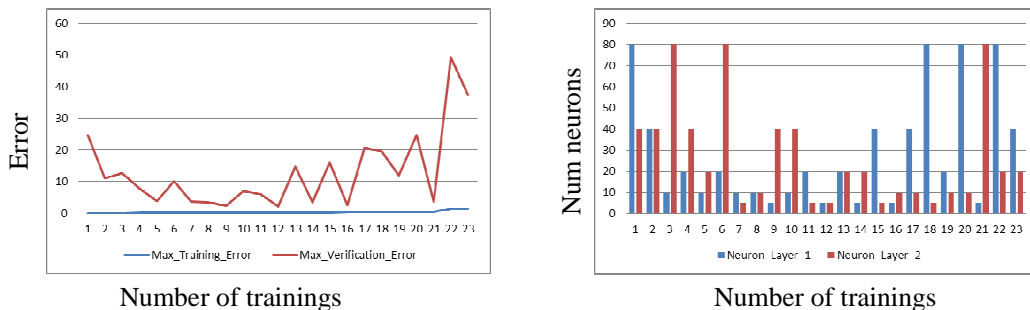


**Figure 31:** Maximum training errors and maximum verification errors on different architecture settings for billet surface temperature at straightening start position (T), trained on 100 training sets.

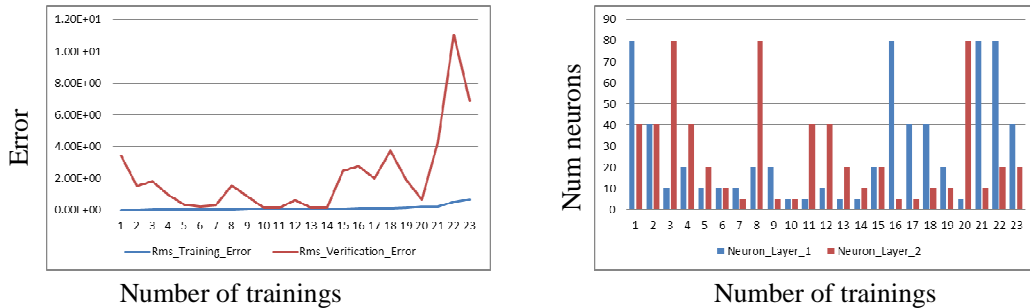


**Figure 32:** Rms training errors and Rms verification errors on different architecture settings for billet surface temperature at straightening start position (T), trained on 100 training sets.

### 4.3.2 Training on 200 Training Sets

#### 4.3.2.1 Metallurgical length (ML)

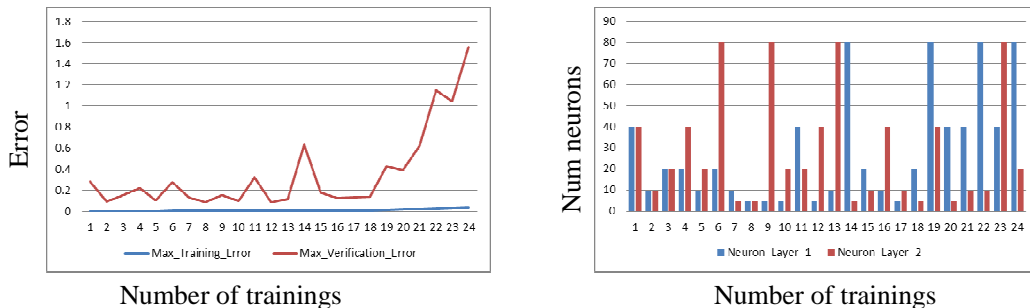


**Figure 33:** Maximum training errors and maximum verification errors on different architecture settings for metallurgical length (ML), trained on 200 training sets.

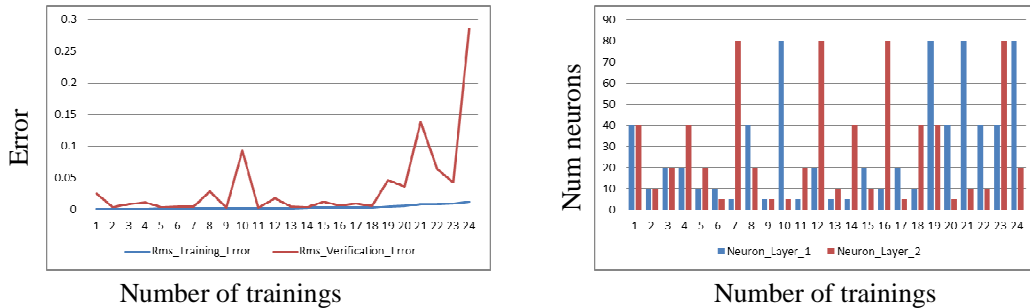


**Figure 34:** Rms training errors and Rms verification errors on different architecture settings for metallurgical length (ML), trained on 200 training sets.

#### 4.3.2.2 Shell Thickness at the End of the Mould (DS)

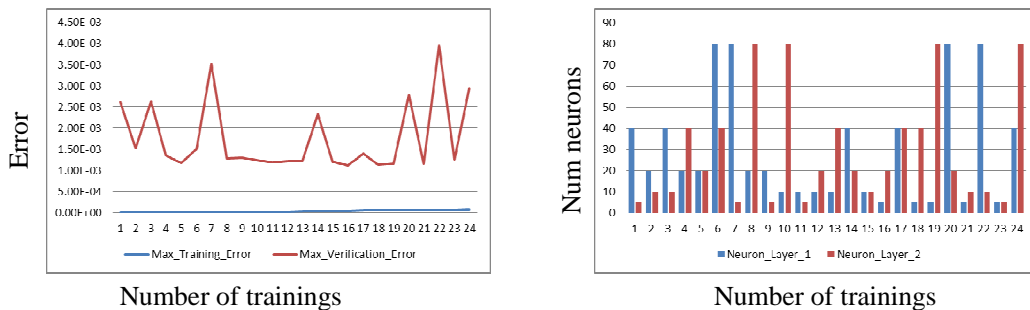


**Figure 35:** Maximum training errors and maximum verification errors on different architecture settings for shell thickness at the end of the mould (DS), trained on 200 training sets.

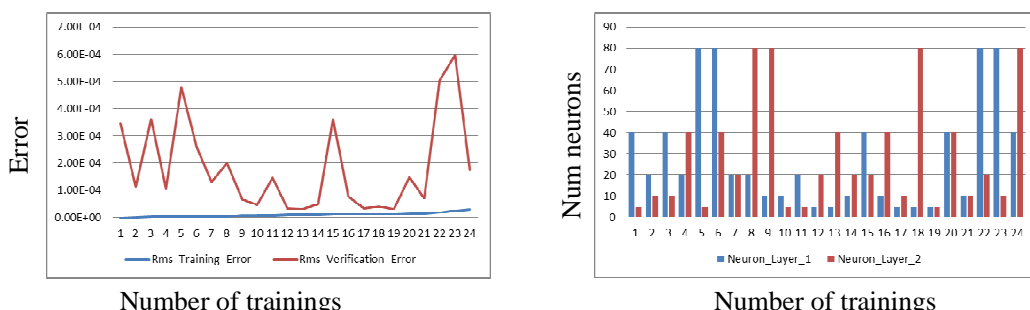


**Figure 36:** Rms training errors and Rms verification errors on different architecture settings for shell thickness at the end of the mould (DS), trained on 200 training sets.

### 4.3.2.3 Billet Surface Temperature at Straightening Start Position (T)

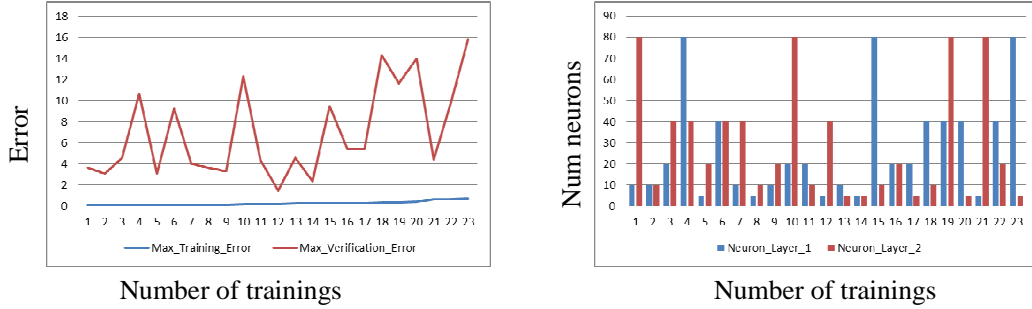


**Figure 37:** Maximum training errors and maximum verification errors on different architecture settings for billet surface temperature at straightening start position (T), trained on 200 training sets.

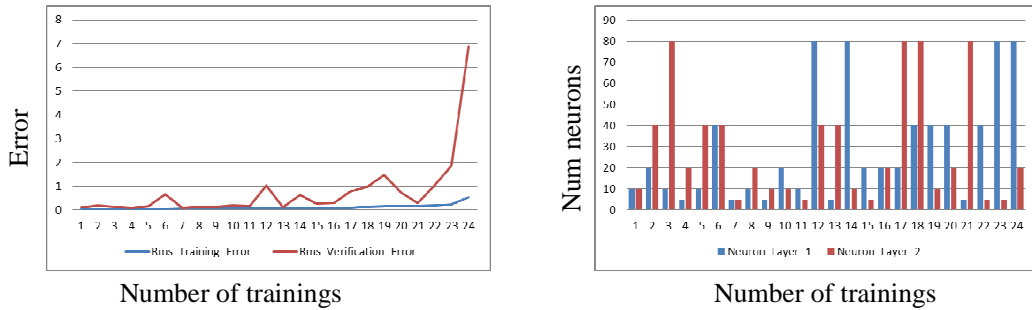


**Figure 38:** Rms training errors and Rms verification errors on different architecture settings for billet surface temperature at straightening start position (T), trained on 200 training sets.

### 4.3.3 Training on 500 Training Sets

#### 4.3.3.1 Metallurgical length (ML)

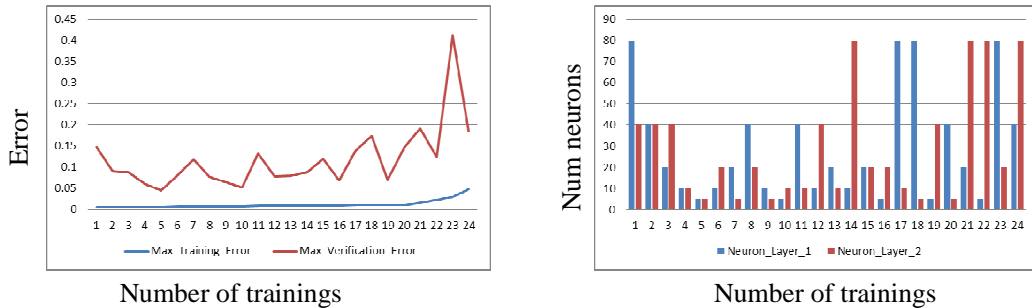


**Figure 39:** Maximum training errors and maximum verification errors on different architecture settings for metallurgical length (ML), trained on 500 training sets.

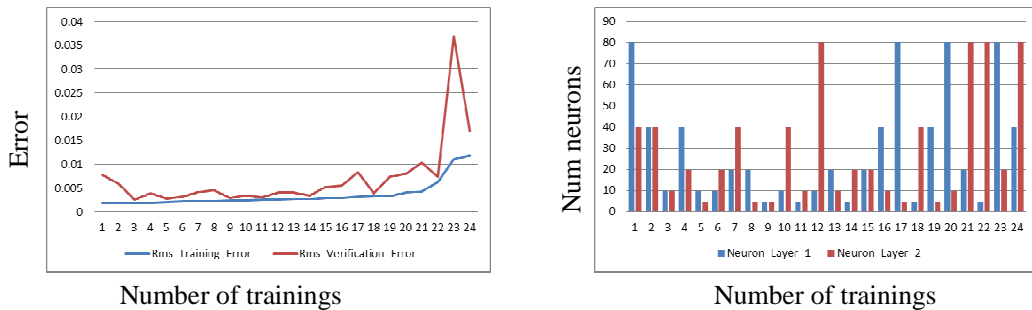


**Figure 40:** Rms training errors and Rms verification errors on different architecture settings for metallurgical length (ML), trained on 500 training sets.

#### 4.3.3.2 Shell Thickness at the End of the Mould (DS)

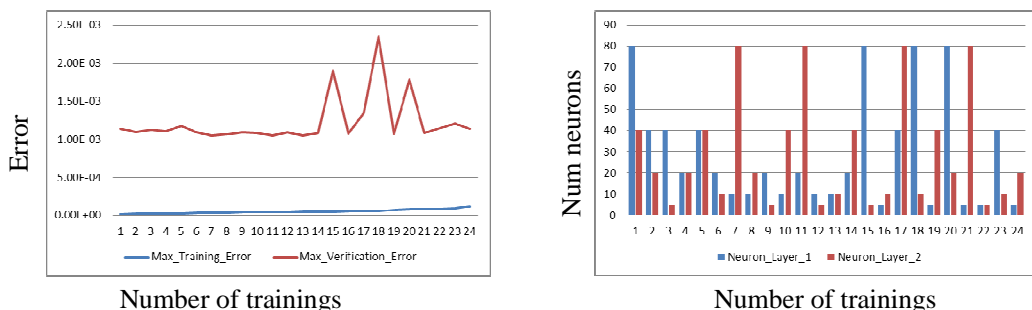


**Figure 41:** Maximum training errors and maximum verification errors on different architecture settings for shell thickness at the end of the mould (DS), trained on 500 training sets.

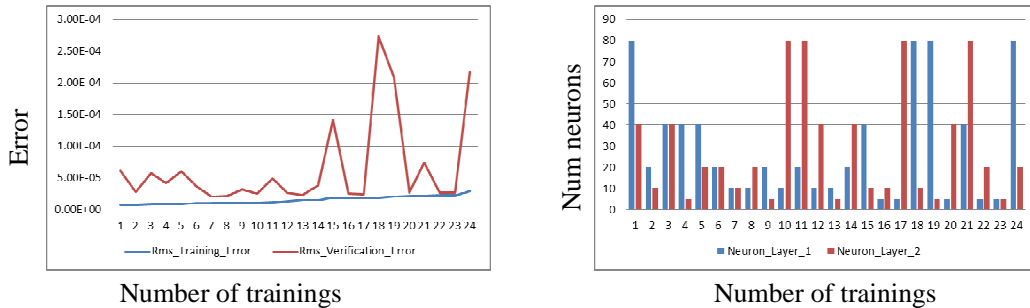


**Figure 42:** Rms training errors and Rms verification errors on different architecture settings for shell thickness at the end of the mould (DS), trained on 500 training sets.

#### 4.3.3.3 Billet Surface Temperature at Straightening Start Position (T)

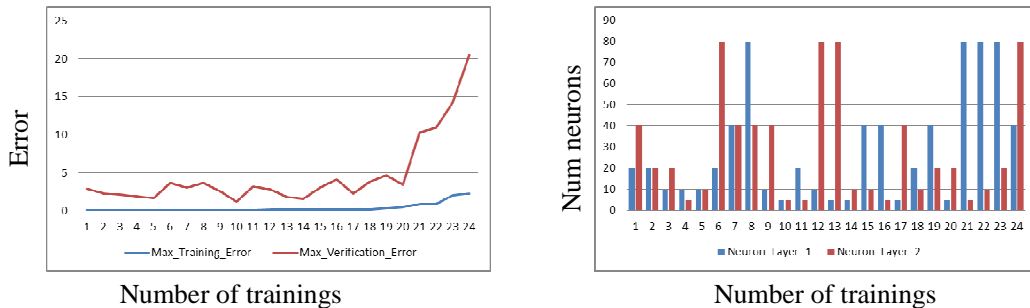


**Figure 43:** Maximum training errors and maximum verification errors on different architecture settings for billet surface temperature at straightening start position (T), trained on 500 training sets.

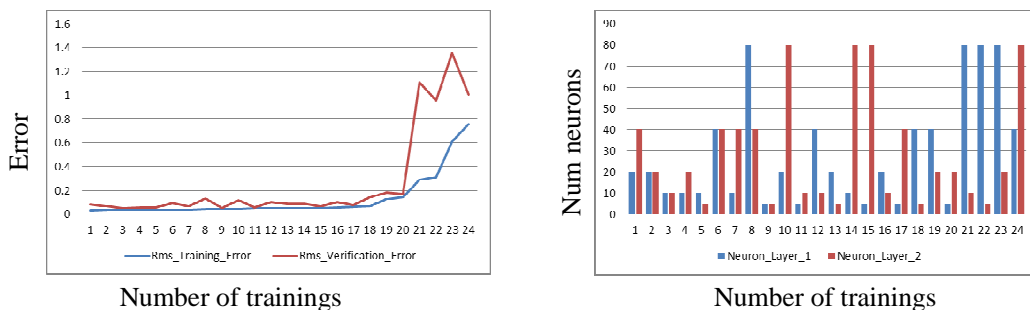


**Figure 44:** Rms training errors and Rms verification errors on different architecture settings for billet surface temperature at straightening start position (T), trained on 500 training sets.

### 4.3.4 Training on 1000 Training Sets

#### 4.3.4.1 Metallurgical length (ML)

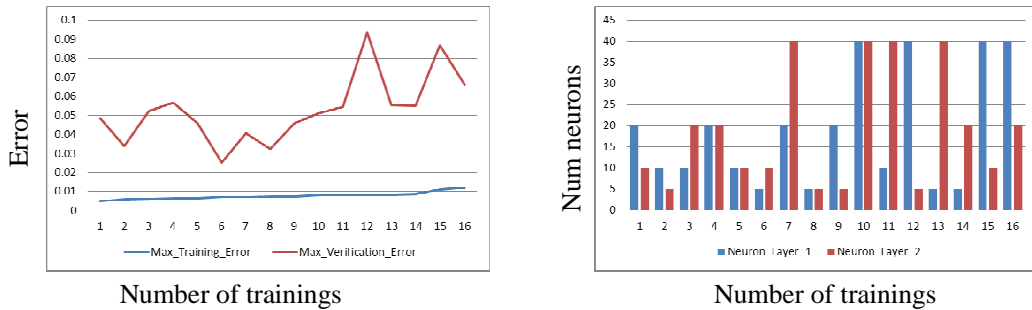


**Figure 45:** Maximum training errors and maximum verification errors on different architecture settings for metallurgical length (ML), trained on 1000 training sets.

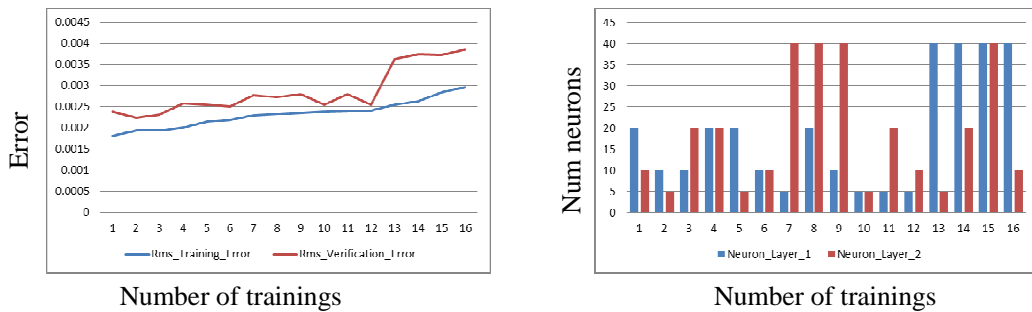


**Figure 46:** Rms training errors and Rms verification errors on different architecture settings for metallurgical length (ML), trained on 1000 training sets.

#### 4.3.4.2 Shell Thickness at the End of the Mould (DS)

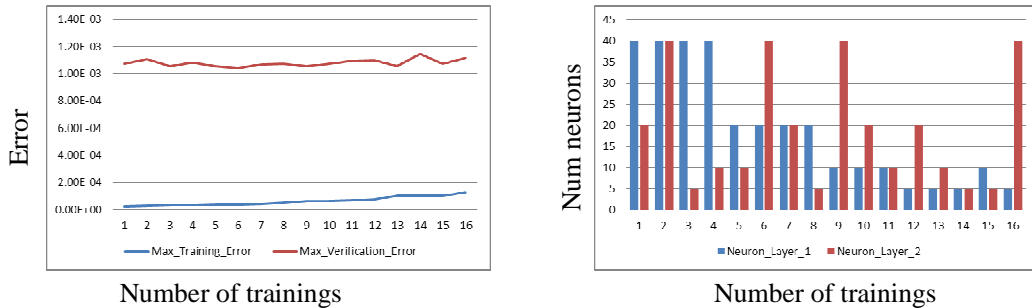


**Figure 47:** Maximum training errors and maximum verification errors on different architecture settings for shell thickness at the end of the mould (DS), trained on 1000 training sets.

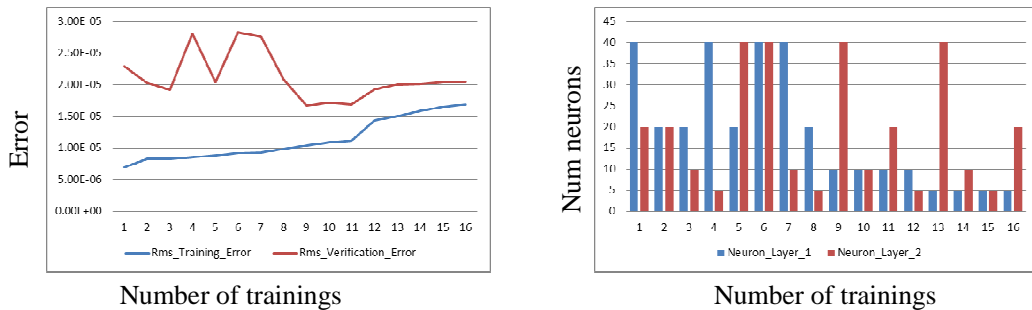


**Figure 48:** Rms training errors and Rms verification errors on different architecture settings for shell thickness at the end of the mould (DS), trained on 1000 training sets.

#### 4.3.4.3 Billet Surface Temperature at Straightening Start Position (T)

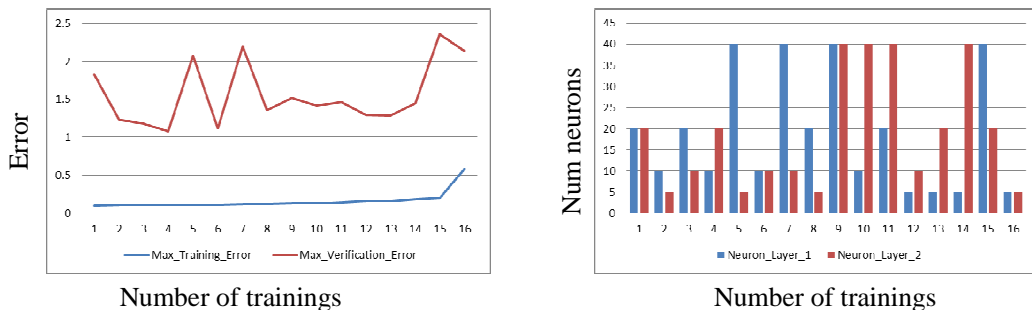


**Figure 49:** Maximum training errors and maximum verification errors on different architecture settings for billet surface temperature at straightening start position (T), trained on 1000 training sets.

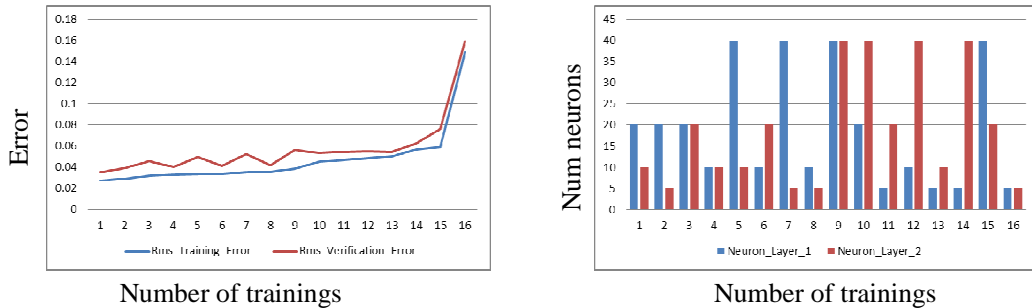


**Figure 50:** Rms training errors and Rms verification errors on different architecture settings for billet surface temperature at straightening start position (T), trained on 1000 training sets.

### 4.3.5 Training on 2000 Training Sets

#### 4.3.5.1 Metallurgical length (ML)

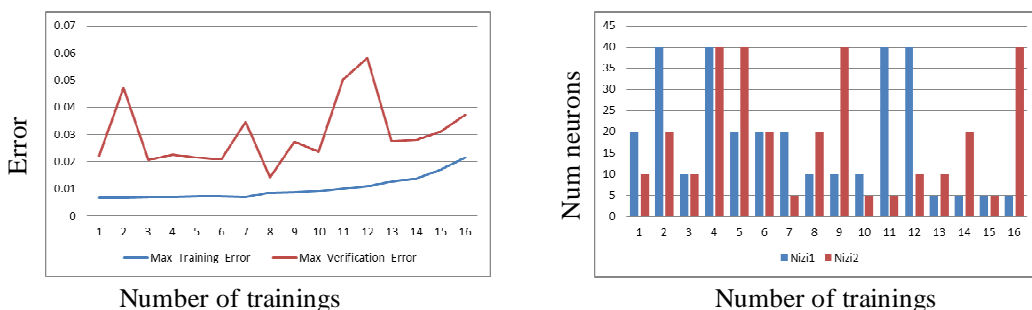


**Figure 51:** Maximum training errors and maximum verification errors on different architecture settings for metallurgical length (ML), trained on 2000 training sets.

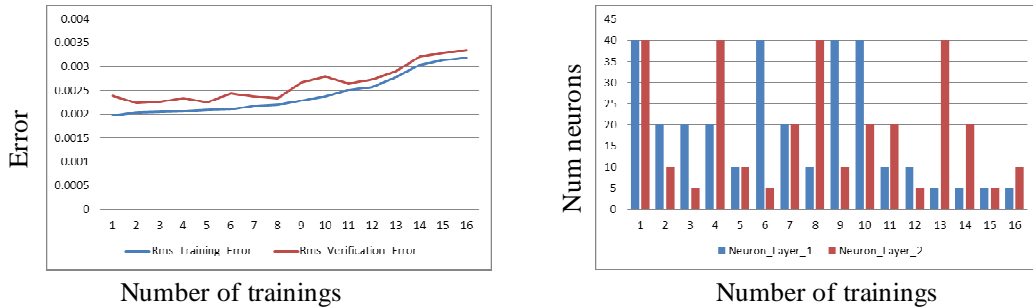


**Figure 52:** Rms training errors and Rms verification errors on different architecture settings for metallurgical length (ML), trained on 2000 training sets.

#### 4.3.5.2 Shell Thickness at the End of the Mould (DS)

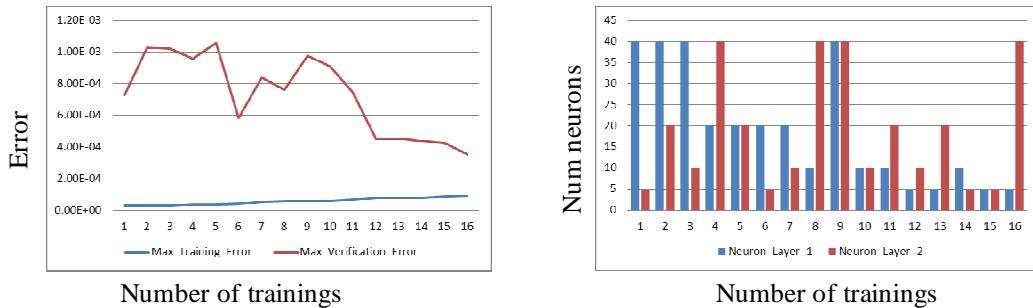


**Figure 53:** Maximum training errors and maximum verification errors on different architecture settings for shell thickness at the end of the mould (DS), trained on 2000 training sets.

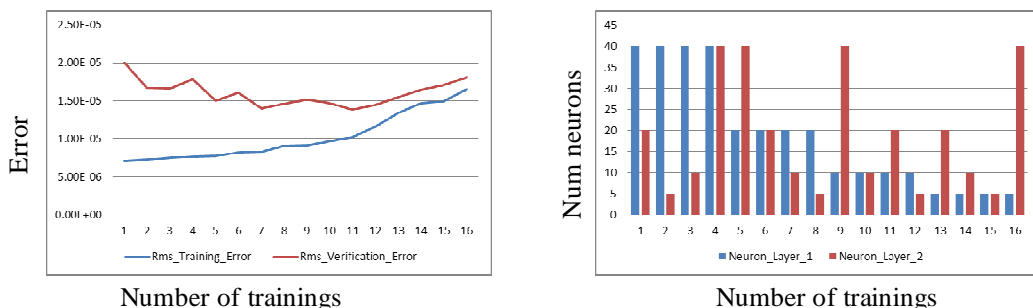


**Figure 54:** Rms training errors and Rms verification errors on different architecture settings for shell thickness at the end of the mould (DS), trained on 2000 training sets.

### 4.3.5.3 Billet Surface Temperature at Straightening Start Position (T)

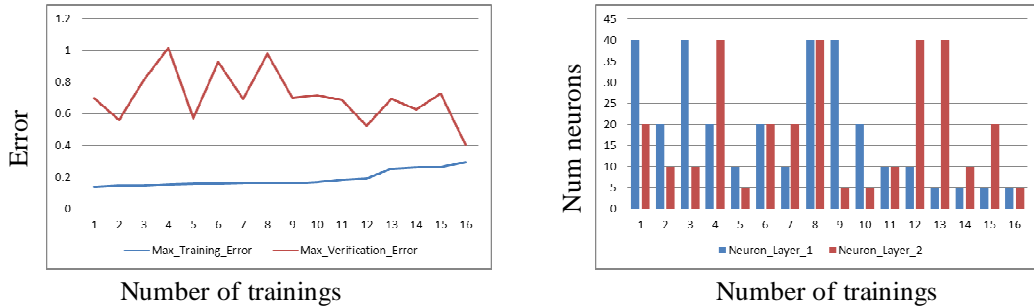


**Figure 55:** Maximum training errors and maximum verification errors on different architecture settings for billet surface temperature at straightening start position (T), trained on 2000 training sets.

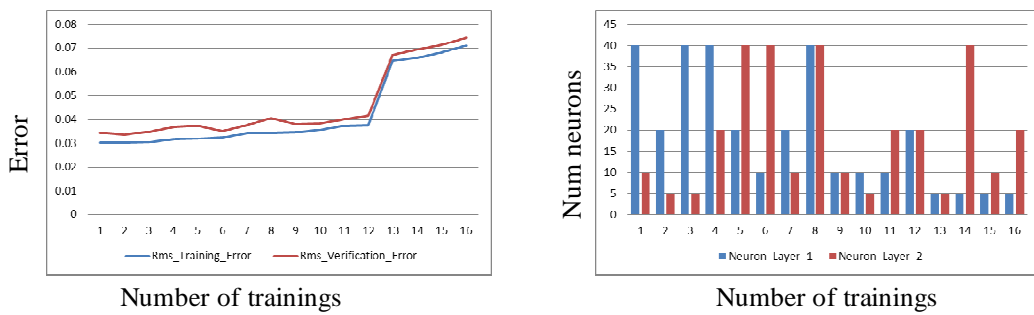


**Figure 56:** Rms training errors and Rms verification errors on different architecture settings for billet surface temperature at straightening start position (T), trained on 2000 training sets.

### 4.3.6 Training on 5000 Training Sets

#### 4.3.6.1 Metallurgical length (ML)

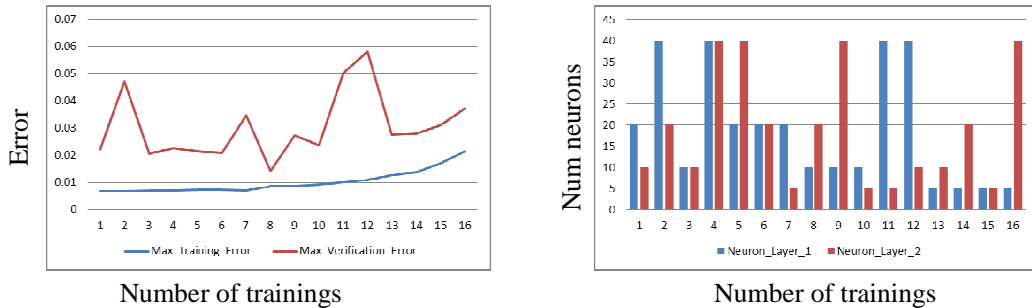


**Figure 57:** Maximum training errors and maximum verification errors on different architecture settings for metallurgical length (ML), trained on 5000 training sets.

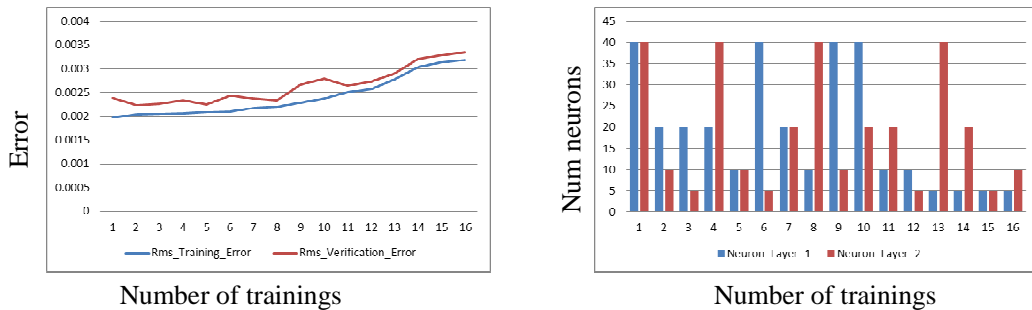


**Figure 58:** Rms training errors and Rms verification errors on different architecture settings for metallurgical length (ML), trained on 5000 training sets.

#### 4.3.6.2 Shell Thickness at the End of the Mould (DS)

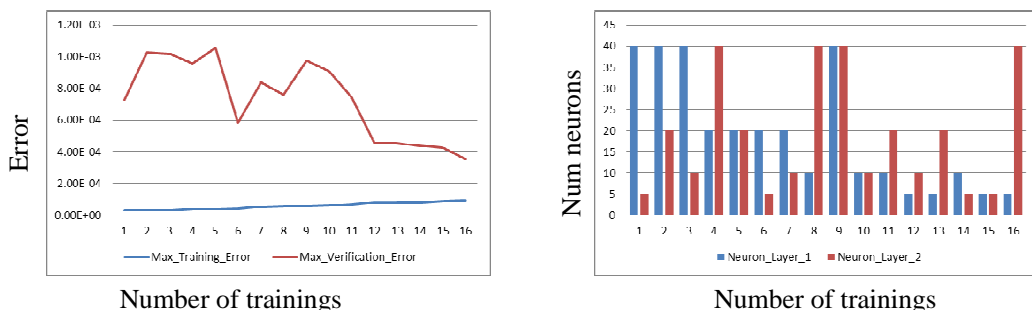


**Figure 59:** Maximum training errors and maximum verification errors on different architecture settings for shell thickness at the end of the mould (DS), trained on 5000 training sets.

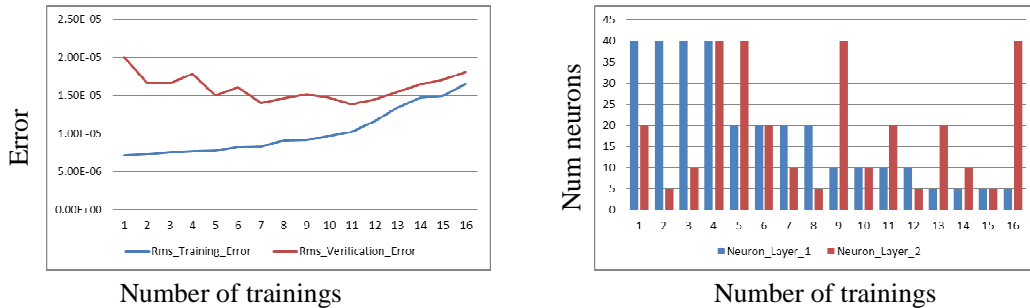


**Figure 60:** Rms training errors and Rms verification errors on different architecture settings for shell thickness at the end of the mould (DS), trained on 5000 training sets.

#### 4.3.6.3 Billet Surface Temperature at Straightening Start Position (T)

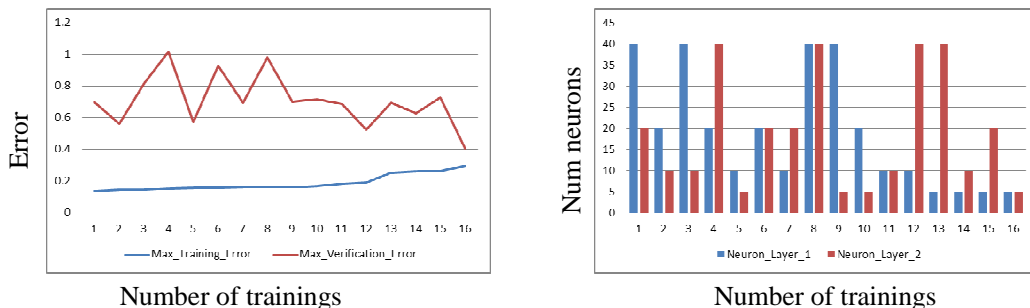


**Figure 61:** Maximum training errors and maximum verification errors on different architecture settings for billet surface temperature at straightening start position (T), trained on 5000 training sets.

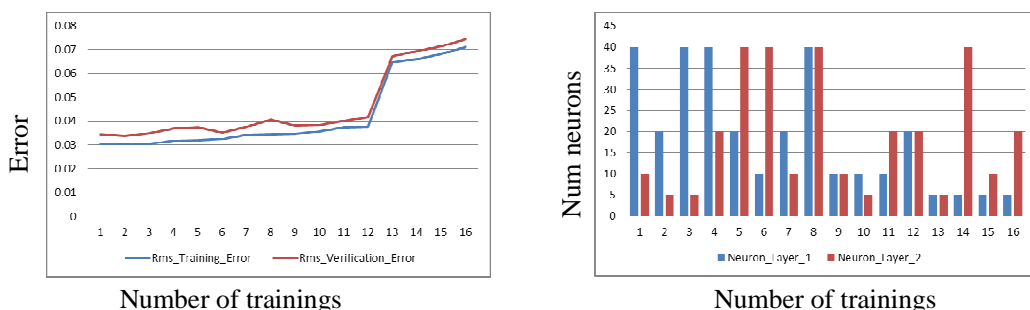


**Figure 62:** Rms training errors and Rms verification errors on different architecture settings for billet surface temperature at straightening start position (T), trained on 5000 training sets.

### 4.3.7 Training on 10000 Training Sets

#### 4.3.7.1 Metallurgical length (ML)

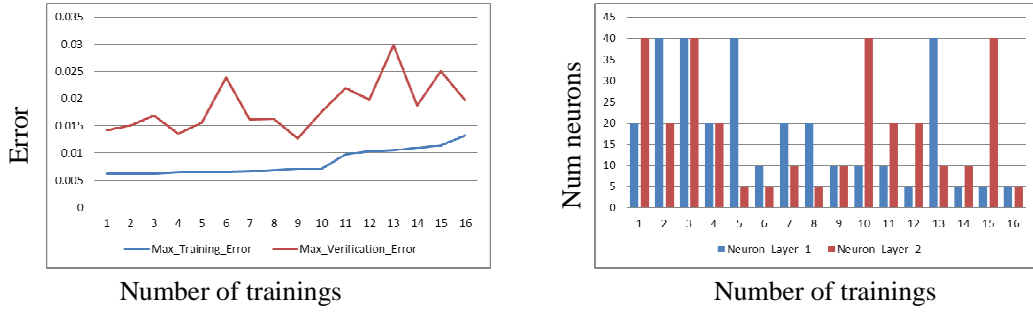


**Figure 63:** Maximum training errors and maximum verification errors on different architecture settings for metallurgical length (ML), trained on 10000 training sets.

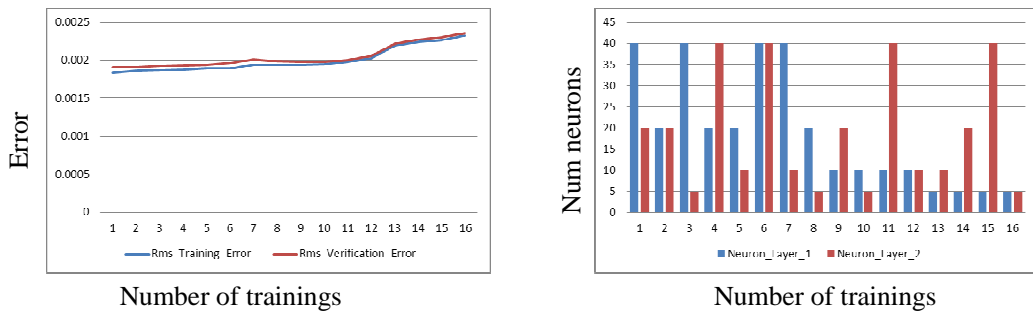


**Figure 64:** Rms training errors and Rms verification errors on different architecture settings for metallurgical length (ML), trained on 10000 training sets.

#### 4.3.7.2 Shell Thickness at the End of the Mould (DS)

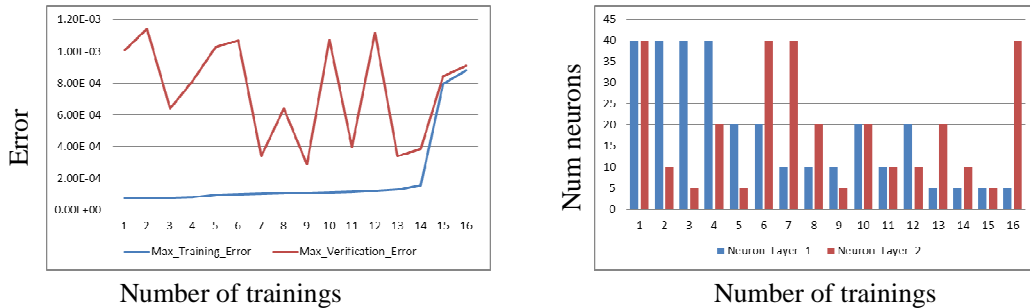


**Figure 65:** Maximum training errors and maximum verification errors on different architecture settings for shell thickness at the end of the mould (DS), trained on 10000 training sets.

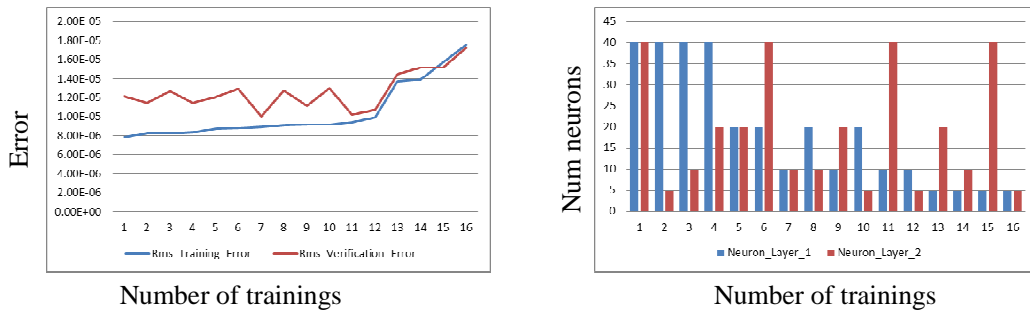


**Figure 66:** Rms training errors and Rms verification errors on different architecture settings for shell thickness at the end of the mould (DS), trained on 10000 training sets.

#### 4.3.7.3 Billet Surface Temperature at Straightening Start Position (T)

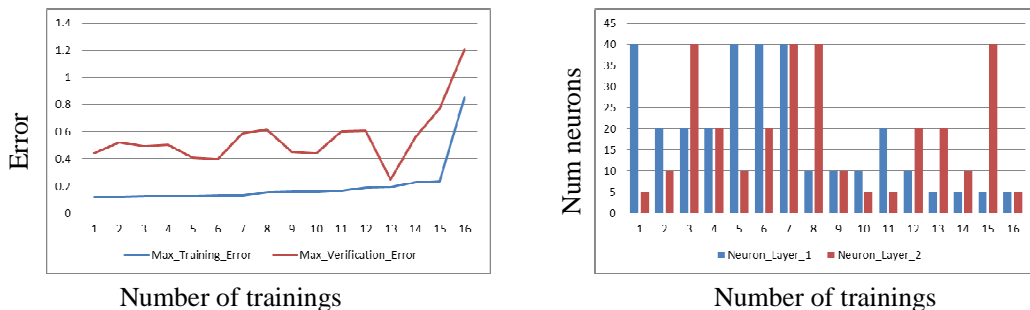


**Figure 67:** Maximum training errors and maximum verification errors on different architecture settings for billet surface temperature at straightening start position (T), trained on 10000 training sets.

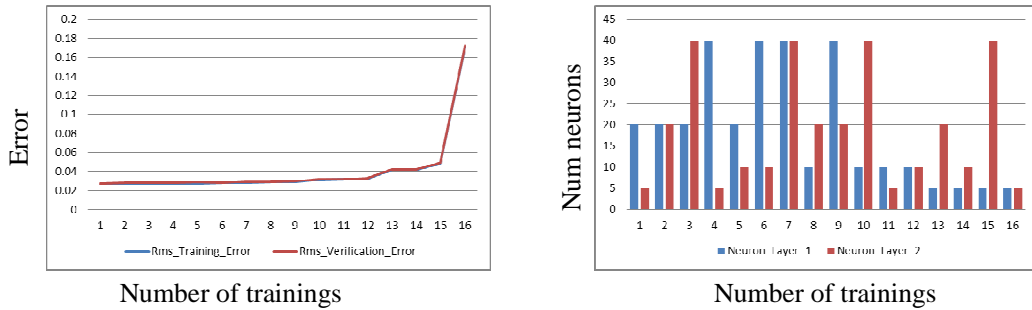


**Figure 68:** Rms training errors and Rms verification errors on different architecture settings for billet surface temperature at straightening start position (T), trained on 10000 training sets.

### 4.3.8 Best Architecture for Different Training Sets

**Table 5:** Best ANN architecture for Max training error.

	TP 100	TP 200	TP 500	TP 1000	TP 2000	TP 5000	TP 10000
Number of hidden layers	2	2	2	2	2	2	2
Number of neurons in hidden layer 1	40	40	80	20	20	20	20
Number of neurons in hidden layer 2	20	40	40	10	10	10	40
Learning rate	0.6	0.6	0.6	0.6	0.6	0.6	0.6
Momentum	0.5	0.5	0.5	0.5	0.5	0.5	0.5
Input safety factor	1.4	1.4	1.4	1.4	1.4	1.4	1.4
Output safety factor	1.4	1.4	1.4	1.4	1.4	1.4	1.4

**Table 6:** Best ANN architecture for Rms training error.

	TP 100	TP 200	TP 500	TP 1000	TP 2000	TP 5000	TP 10000
Number of hidden layers	2	2	2	2	2	2	2
Number of neurons in hidden layer 1	40	40	80	20	40	40	40
Number of neurons in hidden layer 2	20	40	40	10	40	40	20
Learning rate	0.6	0.6	0.6	0.6	0.6	0.6	0.6
Momentum	0.5	0.5	0.5	0.5	0.5	0.5	0.5
Input safety factor	1.4	1.4	1.4	1.4	1.4	1.4	1.4
Output safety factor	1.4	1.4	1.4	1.4	1.4	1.4	1.4

**Table 7:** Best ANN architecture for Max verification error.

	<b>TP 100</b>	<b>TP 200</b>	<b>TP 500</b>	<b>TP 1000</b>	<b>TP 2000</b>	<b>TP 5000</b>	<b>TP 10000</b>
Number of hidden layers	2	2	2	2	2	2	2
Number of neurons in hidden layer 1	5	5	5	5	10	10	10
Number of neurons in hidden layer 2	10	40	5	10	20	20	10
Learning rate	0.6	0.6	0.6	0.6	0.6	0.6	0.6
Momentum	0.5	0.5	0.5	0.5	0.5	0.5	0.5
Input safety factor	1.4	1.4	1.4	1.4	1.4	1.4	1.4
Output safety factor	1.4	1.4	1.4	1.4	1.4	1.4	1.4

**Table 8:** Best ANN architecture for Rms verification error.

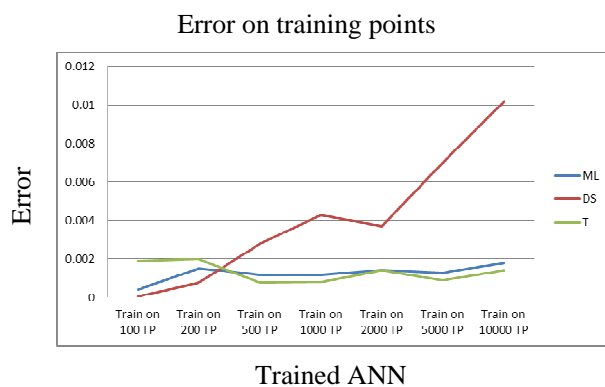
	<b>TP 100</b>	<b>TP 200</b>	<b>TP 500</b>	<b>TP 1000</b>	<b>TP 2000</b>	<b>TP 5000</b>	<b>TP 10000</b>
Number of hidden layers	2	2	2	2	2	2	2
Number of neurons in hidden layer 1	5	5	10	10	10	20	40
Number of neurons in hidden layer 2	10	20	10	5	20	10	20
Learning rate	0.6	0.6	0.6	0.6	0.6	0.6	0.6
Momentum	0.5	0.5	0.5	0.5	0.5	0.5	0.5
Input safety factor	1.4	1.4	1.4	1.4	1.4	1.4	1.4
Output safety factor	1.4	1.4	1.4	1.4	1.4	1.4	1.4

## 5 ERROR ESTIMATION

### 5.1 Maximum Errors on Different Training Sets

**Table 9:** Maximum errors on training points on different data-sets.

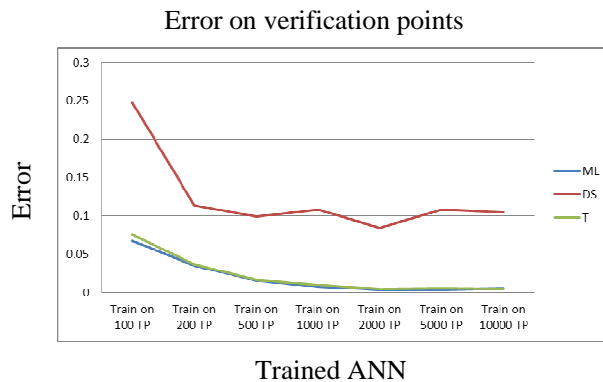
	100 TP	200 TP	500 TP	1000 TP	2000 TP	5000 TP	10000 TP
ML	0.00040	0.0015	0.0012	0.0012	0.0014	0.0013	0.0018
DS	0.00005	0.0008	0.0028	0.0043	0.0037	0.0070	0.0102
T	0.00190	0.0020	0.0008	0.0008	0.0014	0.0009	0.0014



**Figure 69:** Maximum errors on training points on different data-sets.

**Table 10:** Maximum error on verification points on different data-sets.

	100 VP	200 VP	500 VP	1000 VP	2000 VP	5000 VP	10000 VP
ML	0.0680	0.0350	0.0162	0.0079	0.0390	0.0039	0.0053
DS	0.2480	0.1140	0.0990	0.1080	0.0846	0.1080	0.1047
T	0.0760	0.0370	0.0172	0.0106	0.0049	0.0059	0.0045

**Figure 70:** Maximum errors on verification points on different data-sets.

## 6 TRAINING ANN ON OPTIMAL TRAINING SETS

**Table 11:** Best ANN settings and architecture.

Name	Value
Number of training sets	2000
Number of hidden layers	2
Number of neurons in hidden layer 1	20
Number of neurons in hidden layer 2	10
Maximum number of epochs	150.000
Learning rate	0.6
Momentum	0.5
Input safety factor	1.4
Output safety factor	1.4

### 6.1 Error Estimation

#### 6.1.1 Metallurgical Length (ML)

Relative errors for metallurgical length (ML) are represented in Figure 71 for training points and Figure 72 for verification points.

### 6.1.1.1 Errors on Training Points

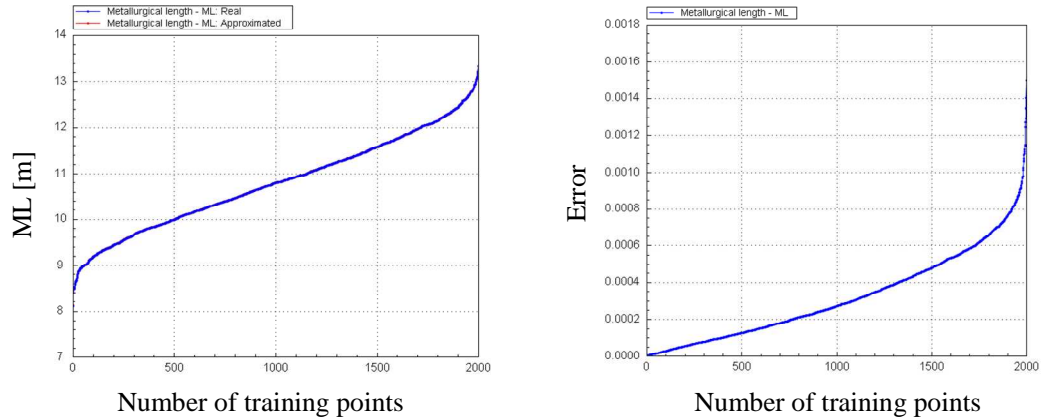


**Figure 71:** Approximation for metallurgical length (ML) in training points. Training points are represented by dots. Left: real elongation values. Right: relative error in training points.

### 6.1.1.2 Errors on Verification Points

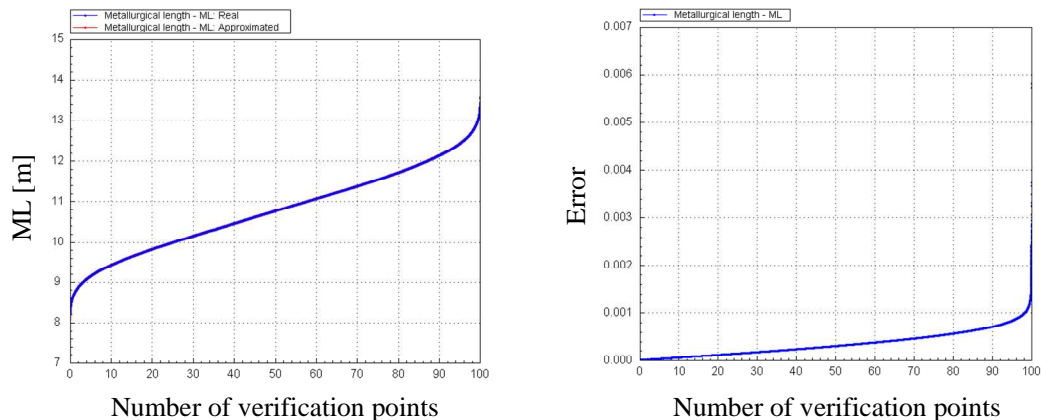


**Figure 72:** Approximation for metallurgical length (ML) in verification points. Verification points are represented by dots. Left: real elongation values. Right: relative error in verification points.

## 6.1.2 Shell Thickness at the end of the Mould (DS)

Relative errors for shell thickness at the end of the mould (DS) are represented in Figure 73 for training points and Figure 74 for verification points.

### 6.1.2.1 Errors on Training Points

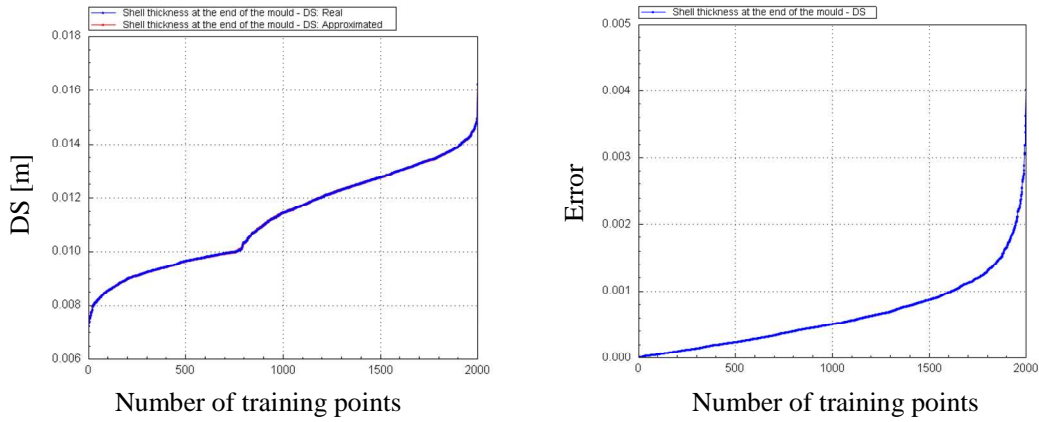


**Figure 73:** Approximation for shell thickness at the end of the mould (DS) in training points. Training points are represented by dots. Left: real tensile strength values. Right: relative error in training points.

### 6.1.2.2 Errors on Verification Points

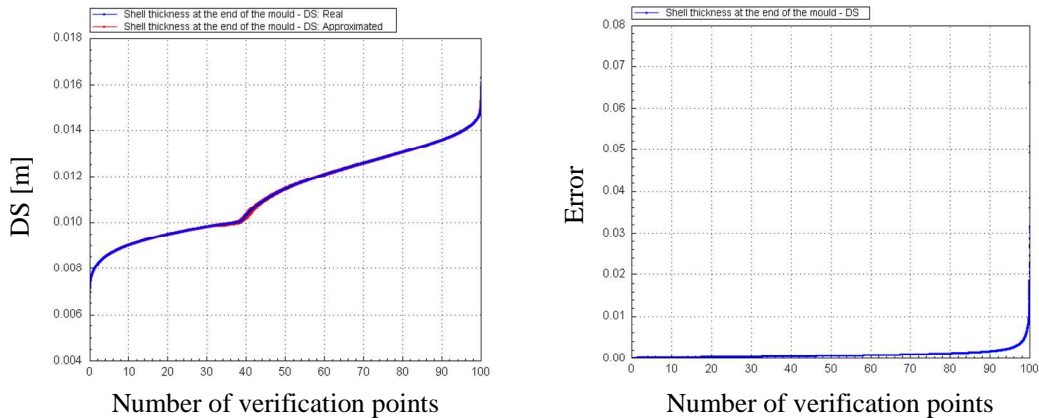


**Figure 74:** Approximation for shell thickness at the end of the mould (DS) in verification points. Verification points are represented by dots. Left: real tensile strength values. Right: relative error in verification points.

### 6.1.3 Billet Surface Temperature at Straightening Start Position (T)

Relative errors for billet surface temperature at straightening start position (T) are represented in Figure 75 for training points and Figure 76 for verification points.

### 6.1.3.1 Errors on Training Points

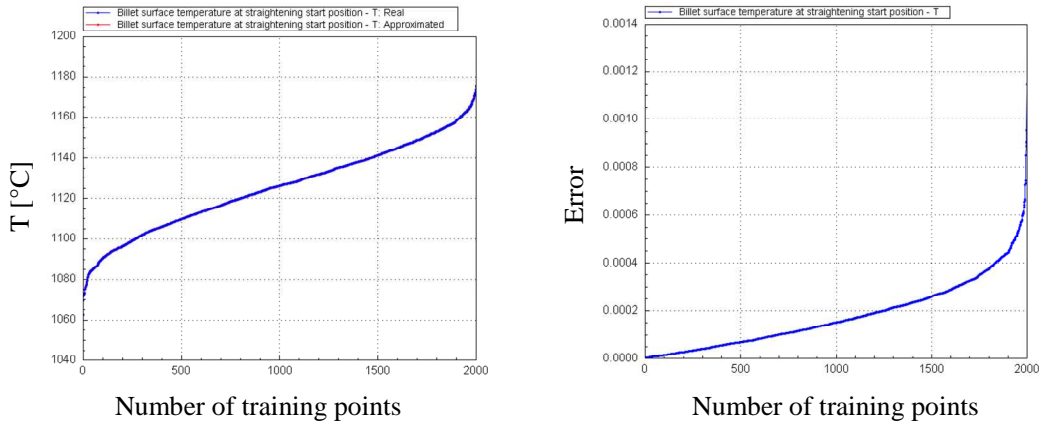


**Figure 75:** Approximation for billet surface temperature at straightening start position ( $T$ ) in training points. Training points are represented by dots. Left: real yield stress values. Right: relative error in training points.

### 6.1.3.2 Errors on Verification Points

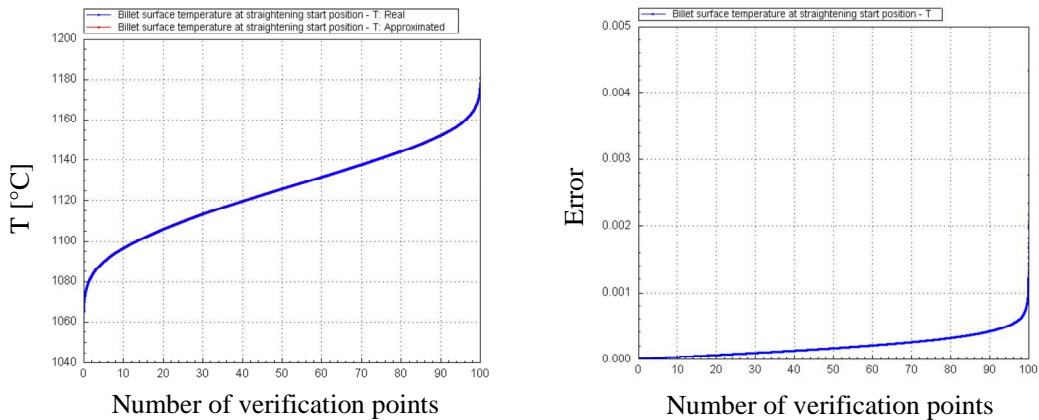


**Figure 76:** Approximation for billet surface temperature at straightening start position ( $T$ ) in verification points. Verification points are represented by dots. Left: real yield stress values. Right: relative error in verification points.

## 6.2 Parametric studies

After performing error estimation tests, some parametric studies were performed. With these parametric tests we try to determine the accuracy of the ANN and also verify dependences between parameters.

### 6.2.1 Center Point

In this study we calculated one center point from training data set and one point from verification data set. Center point for training point was defined as:

$$\mathbf{r}_T = \frac{\sum_{i \in I_T} (\mathbf{p}_i)}{N_T}, \quad (1)$$

while center point for verification set was defined as,

$$\mathbf{r}_V = \frac{\sum_{i \in I_V} (\mathbf{p}_i)}{N_V}. \quad (2)$$

In each chosen point we varied one parameter, while other parameters were fixed. Parameter was varied within the range defined by the minimum and maximum value of that parameter over all dataset used in training. These kind of tests help us find out how the change of one parameter, influences on final material properties. We performed these tests for all 34 input parameters. The influences are shown from Figure 77 to Figure 94.

#### 6.2.1.1 Metallurgical Length (ML)

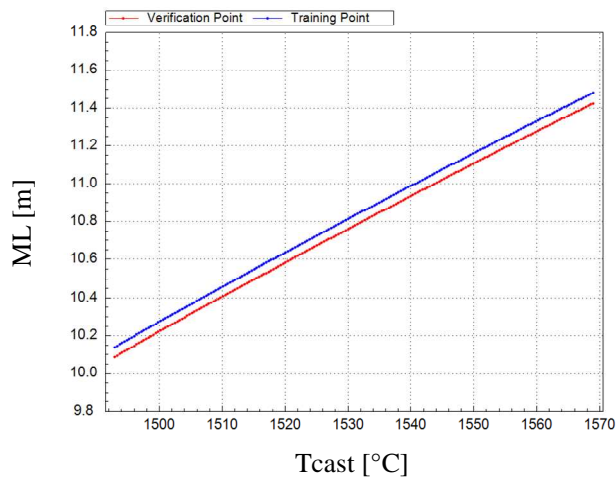


**Figure 77:** Metallurgical length as a function of the casting temperature, calculated by the ANN model on centered verification point (red line) and centered training point (blue line).

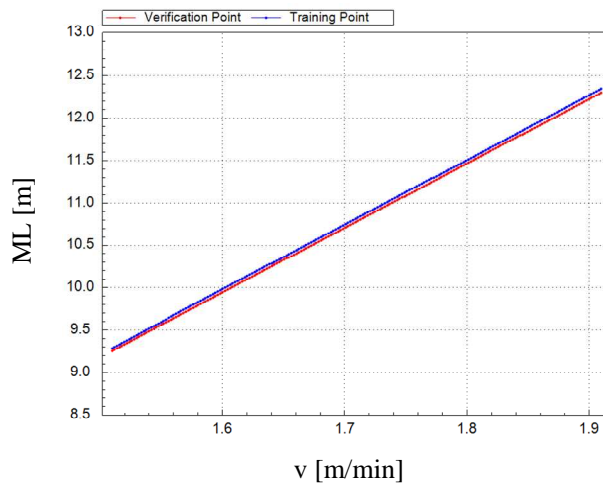


**Figure 78:** Metallurgical length as a function of the casting speed, calculated by the ANN model on centered verification point (red line) and centered training point (blue line).

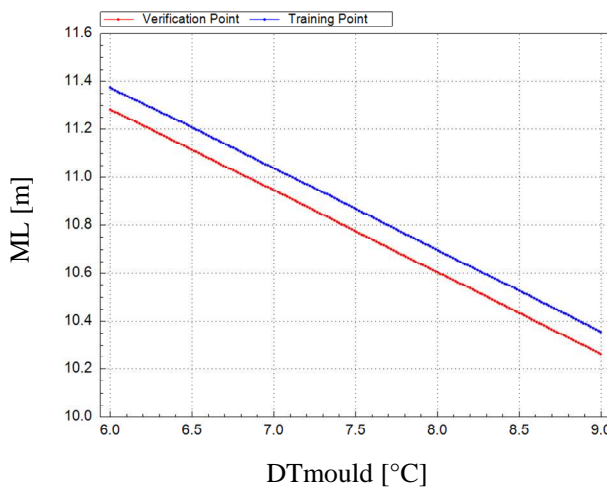


**Figure 79:** Metallurgical length as a function of the temperature difference of cooling water in the mould, calculated by the ANN model on centered verification point (red line) and centered training point (blue line).

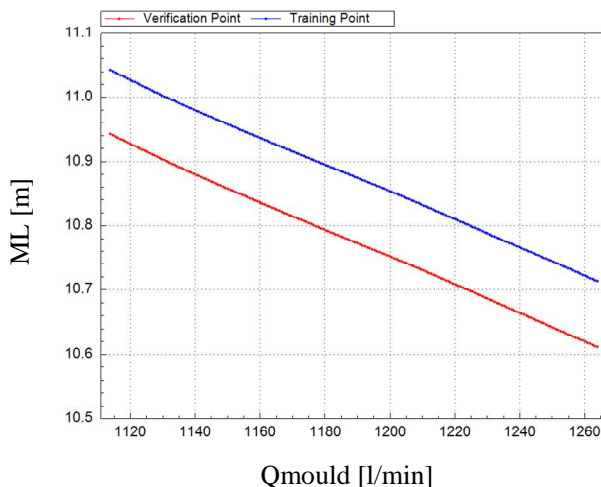


**Figure 80:** Metallurgical length as a function of the cooling flow rate in the mould, calculated by the ANN model on centered verification point (red line) and centered training point (blue line).

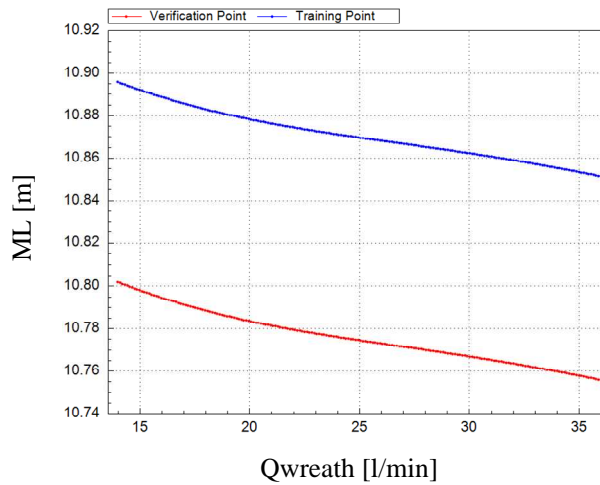


**Figure 81:** Metallurgical length as a function of the cooling flow rate in wreath spray system, calculated by the ANN model on centered verification point (red line) and centered training point (blue line).

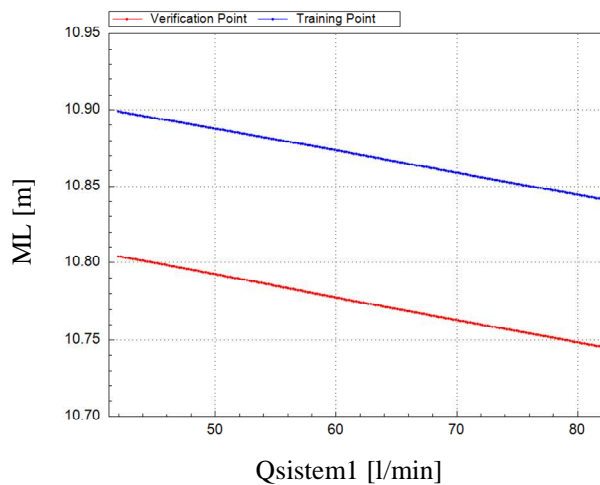


**Figure 82:** Metallurgical length as a function of the cooling flow rate in 1st spray system, calculated by the ANN model on centered verification point (red line) and centered training point (blue line).

### 6.2.1.2 Shell Thickness at the End of the Mould (DS)

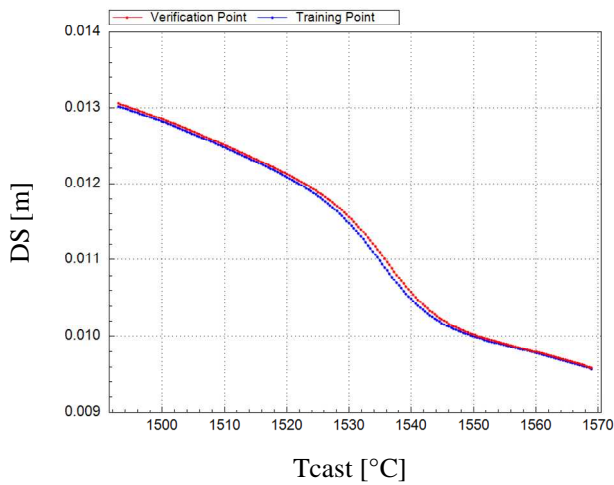


**Figure 83:** Shell thickness at the end of the mould as a function of the casting temperature, calculated by the ANN model on centered verification point (red line) and centered training point (blue line).

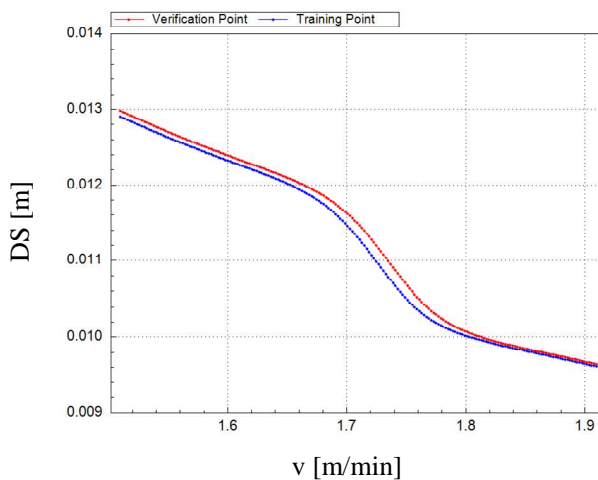


**Figure 84:** Shell thickness at the end of the mould as a function of the casting speed, calculated by the ANN model on centered verification point (red line) and centered training point (blue line).

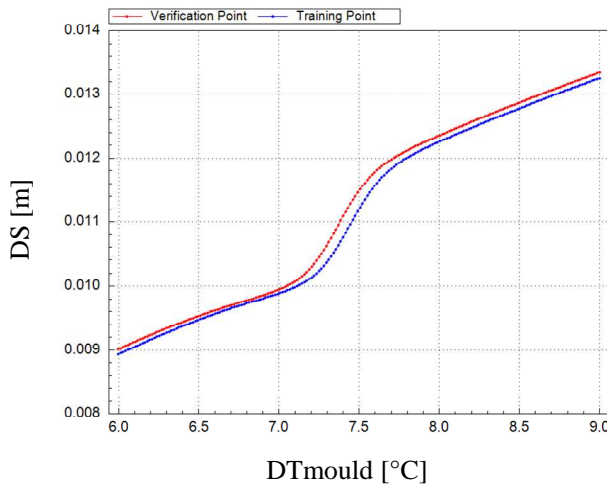


**Figure 85:** Shell thickness at the end of the mould as a function of the temperature difference of cooling water in the mould, calculated by the ANN model on centered verification point (red line) and centered training point (blue line).

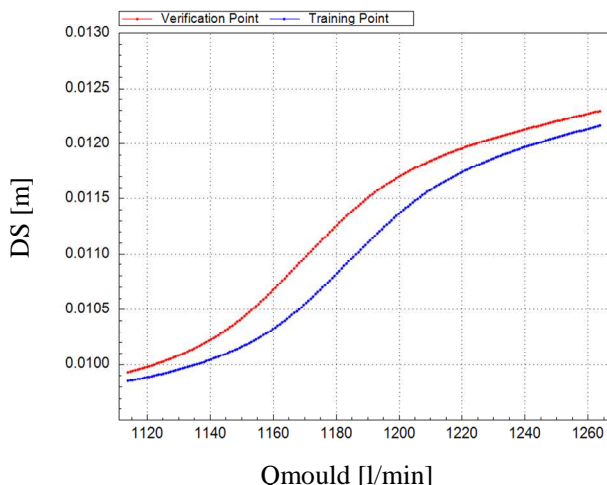


**Figure 86:** Shell thickness at the end of the mould as a function of the cooling flow rate in the mould, calculated by the ANN model on centered verification point (red line) and centered training point (blue line).

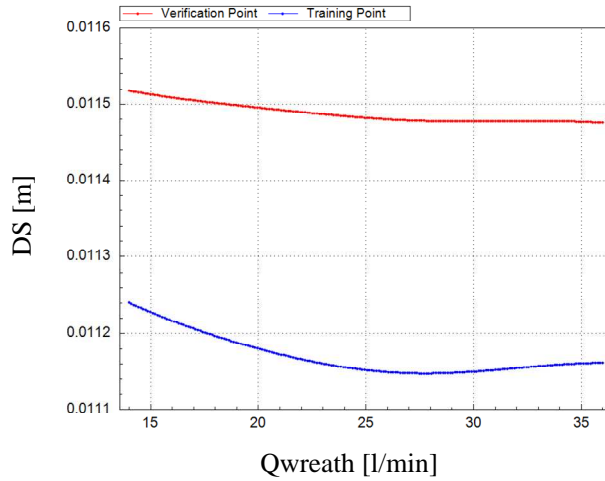


**Figure 87:** Shell thickness at the end of the mould as a function of the cooling flow rate in wreath spray system, calculated by the ANN model on centered verification point (red line) and centered training point (blue line).

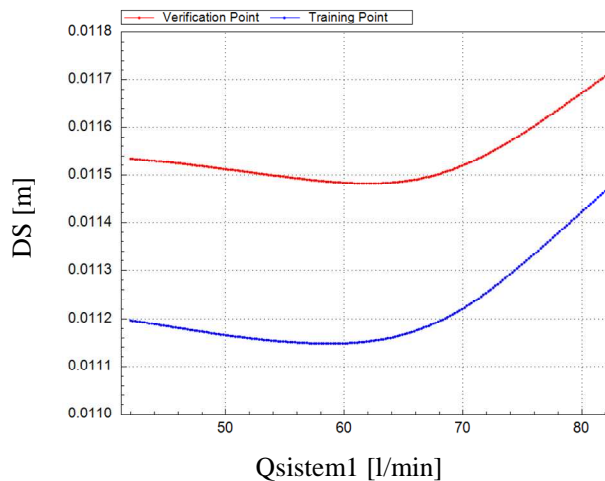


**Figure 88:** Shell thickness at the end of the mould as a function of the cooling flow rate in 1st spray system, calculated by the ANN model on centered verification point (red line) and centered training point (blue line).

### 6.2.1.3 Billet Surface Temperature at Straightening Start Position (T)

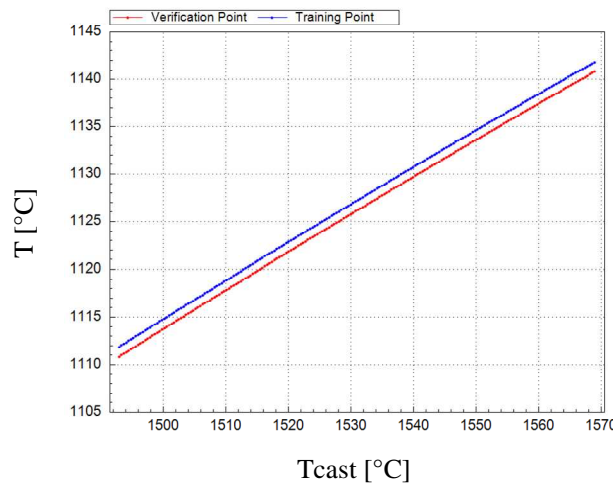


**Figure 89:** Billet surface temperature at straightening start position as a function of the casting temperature, calculated by the ANN model on centered verification point (red line) and centered training point (blue line).

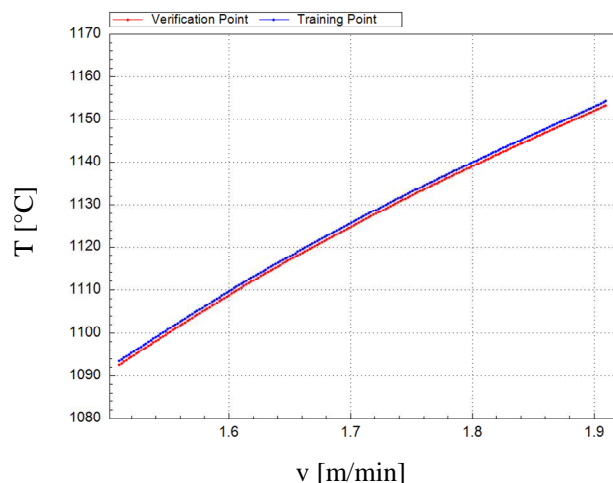


**Figure 90:** Billet surface temperature at straightening start position as a function of the casting speed, calculated by the ANN model on centered verification point (red line) and centered training point (blue line).

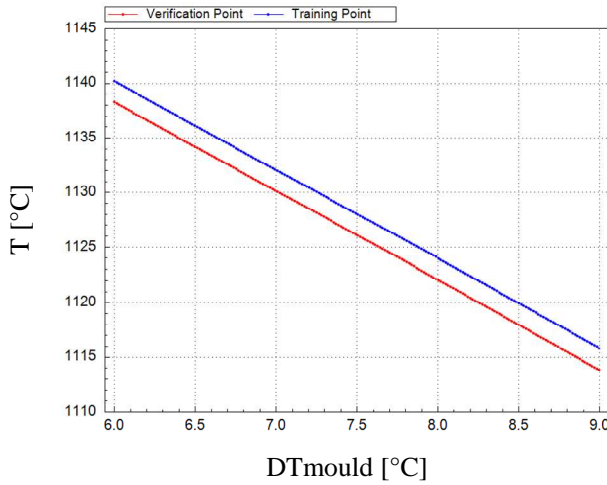


**Figure 91:** Billet surface temperature at straightening start position as a function of the temperature difference of cooling water in the mould, calculated by the ANN model on centered verification point (red line) and centered training point (blue line).

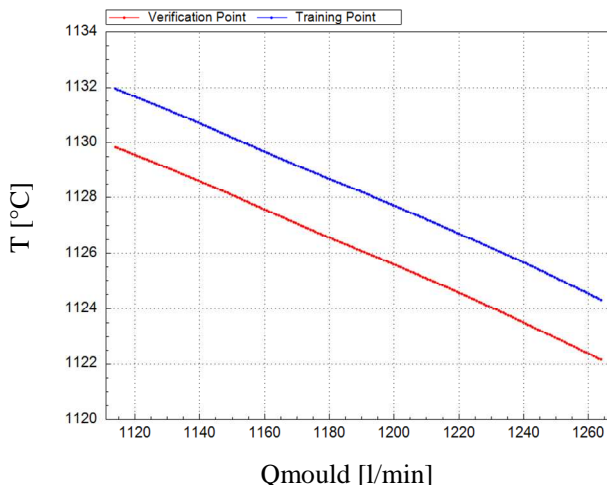


**Figure 92:** Billet surface temperature at straightening start position as a function of the cooling flow rate in the mould, calculated by the ANN model on centered verification point (red line) and centered training point (blue line).

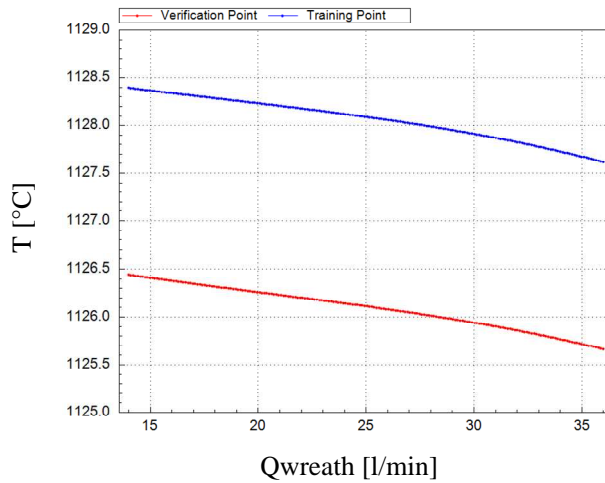


**Figure 93:** Billet surface temperature at straightening start position as a function of the cooling flow rate in wreath spray system, calculated by the ANN model on centered verification point (red line) and centered training point (blue line).

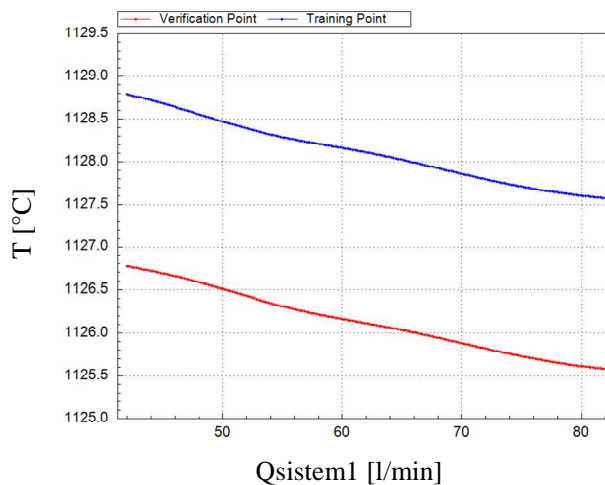


**Figure 94:** Billet surface temperature at straightening start position as a function of the cooling flow rate in 1st spray system, calculated by the ANN model on centered verification point (red line) and centered training point (blue line).

## 6.2.2 Points on Line

We chose two points ( $\mathbf{p}_I, \mathbf{p}_F$ ) from the training data-set and from verification data-set.  $\mathbf{p}_I$  represents initial point with minimum parameters from elected data-set, and  $\mathbf{p}_F$  represents final point, with maximum parameters from that data-set. Then we took a certain number of equally spaced points on the line segment between these two points (including the chosen points). The effects of variation of certain parameters were done for all points and are represented from Figure 95 to Figure 112. The intermediate points  $\mathbf{p}_j$  were calculated according to

$$\mathbf{p}_j = \mathbf{p}_I + (\mathbf{p}_F - \mathbf{p}_I) \frac{j}{n+1}; \quad j = 0, 1, 2, \dots, n+1, \quad (3)$$

where  $j$  is the number of the intermediate points.

### 6.2.2.1 Metallurgical Length (ML)

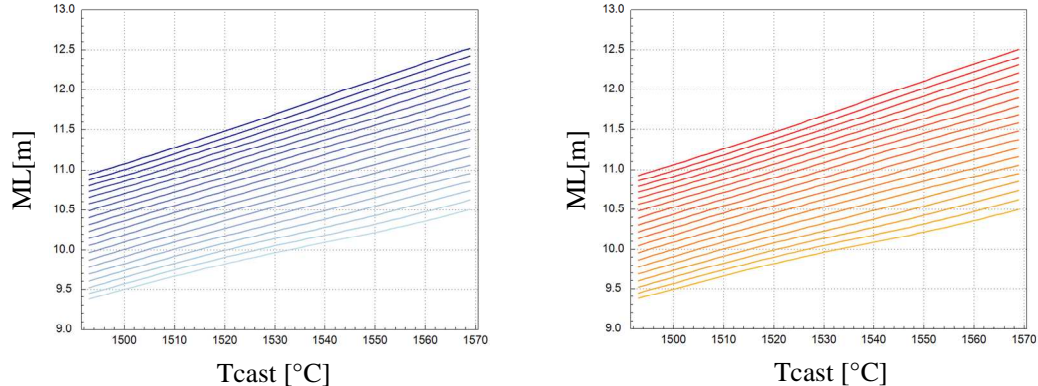


**Figure 95:** Metallurgical length as a function of the casting temperature, calculated by the ANN model in two points from the data set, and for 18 other points on the line between them. Left: training data set. Right: verification data set.

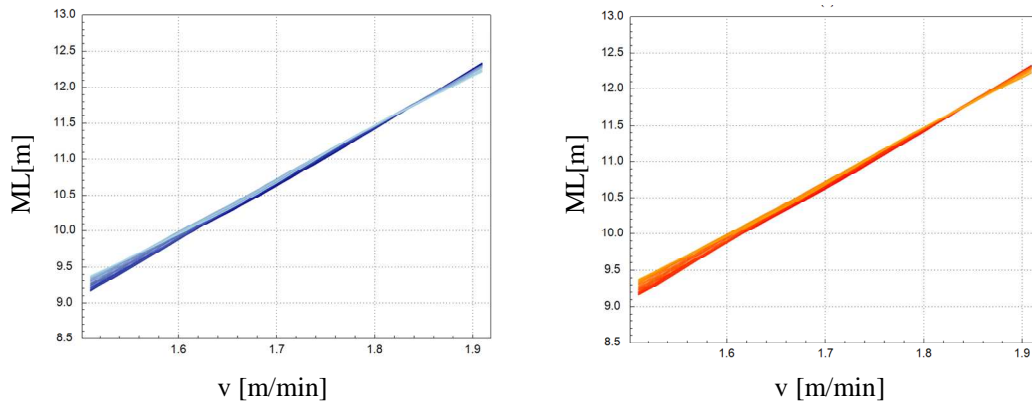


**Figure 96:** Metallurgical length as a function of the casting speed, calculated by the ANN model on centered verification point (red line) and centered training point (blue line).

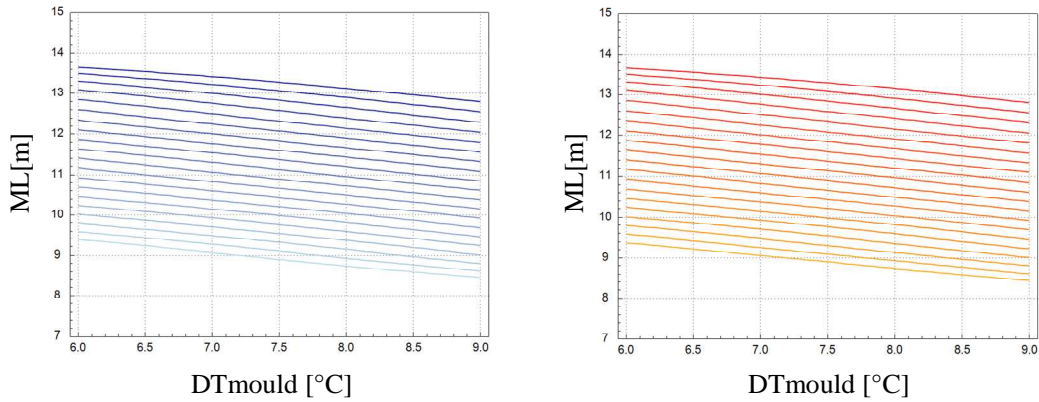


**Figure 97:** Metallurgical length as a function of the temperature difference of cooling water in the mould, calculated by the ANN model on centered verification point (red line) and centered training point (blue line).

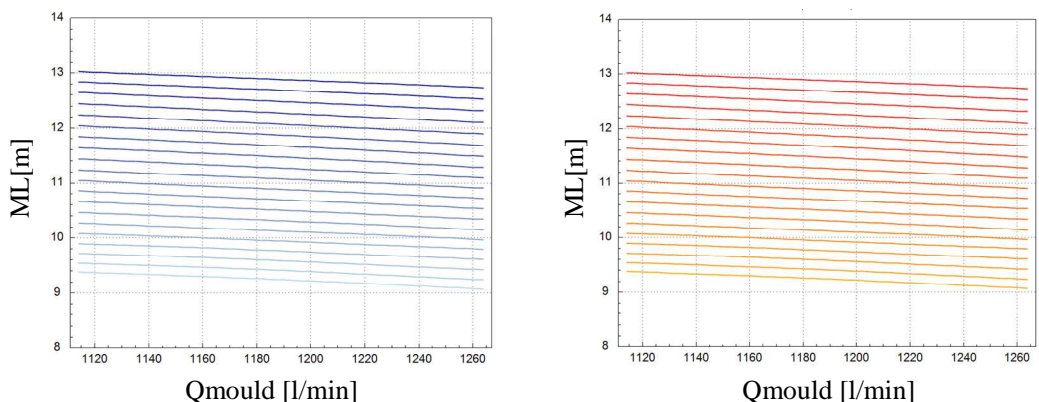


**Figure 98:** Metallurgical length as a function of the cooling flow rate in the mould, calculated by the ANN model on centered verification point (red line) and centered training point (blue line).

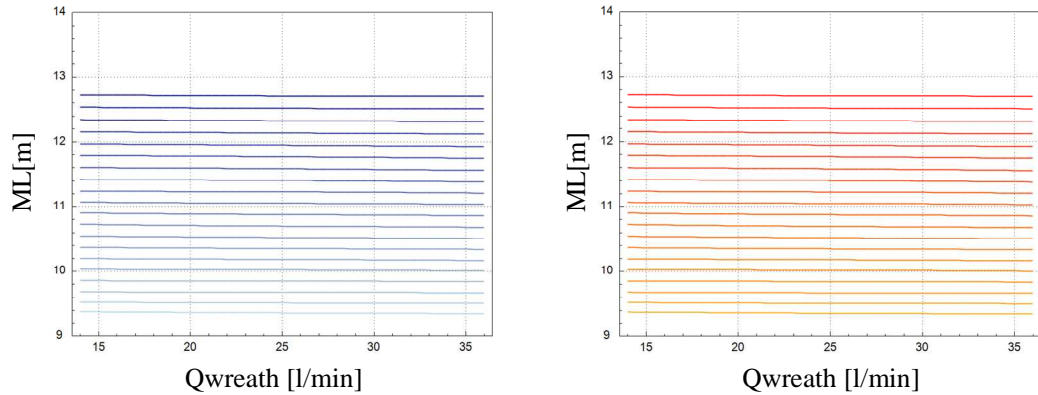


**Figure 99:** Metallurgical length as a function of the cooling flow rate in wreath spray system, calculated by the ANN model on centered verification point (red line) and centered training point (blue line).

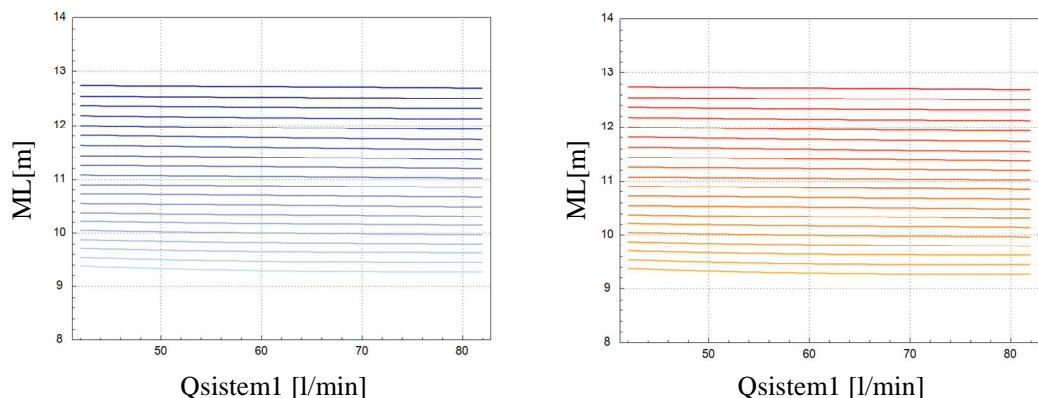


**Figure 100:** Metallurgical length as a function of the cooling flow rate in 1st spray system, calculated by the ANN model on centered verification point (red line) and centered training point (blue line).

### 6.2.2.2 Shell Thickness at the End of the Mould (DS)

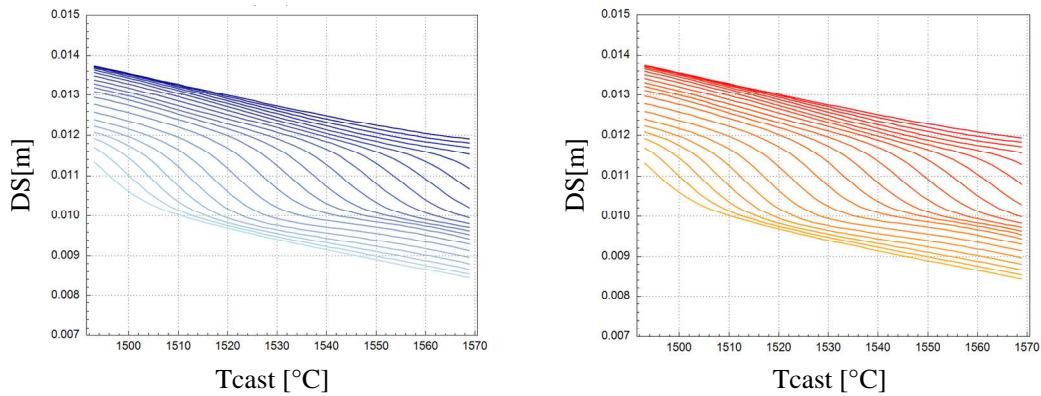


**Figure 101:** Shell thickness at the end of the mould as a function of the casting temperature, calculated by the ANN model in two points from the data set, and for 18 other points on the line between them. Left: training data set. Right: verification data set.

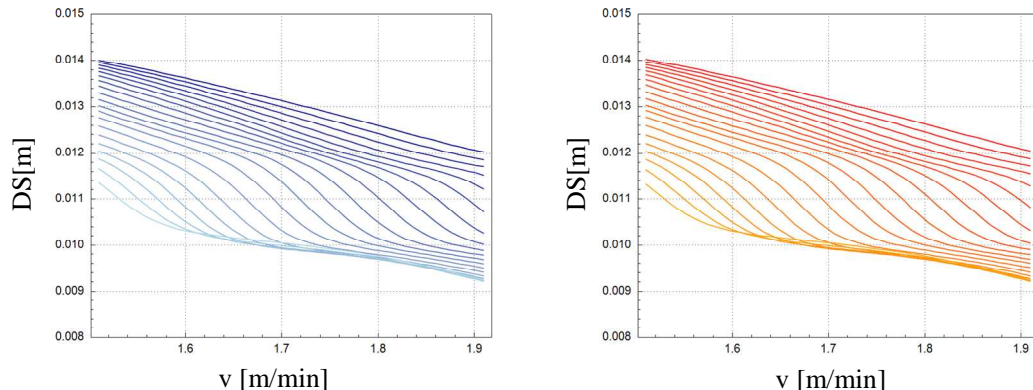


**Figure 102:** Shell thickness at the end of the mould as a function of the casting speed, calculated by the ANN model on centered verification point (red line) and centered training point (blue line).

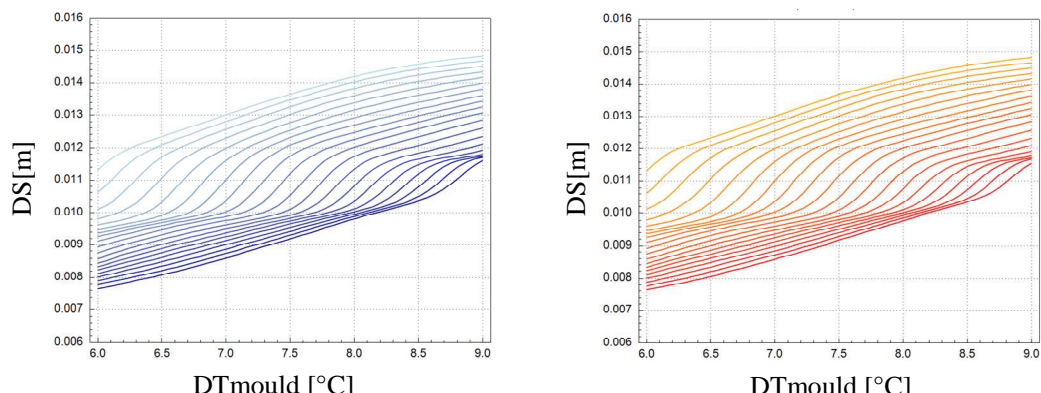


**Figure 103:** Shell thickness at the end of the mould as a function of the temperature difference of cooling water in the mould, calculated by the ANN model on centered verification point (red line) and centered training point (blue line).

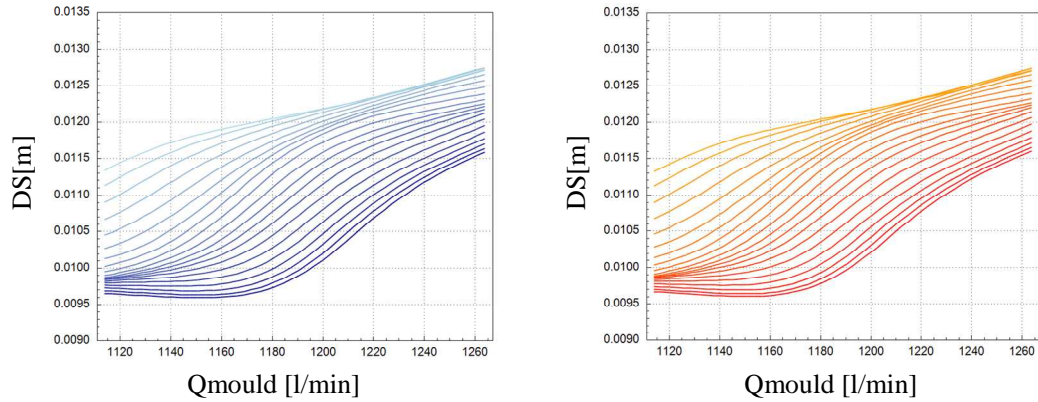


**Figure 104:** Shell thickness at the end of the mould as a function of the cooling flow rate in the mould, calculated by the ANN model on centered verification point (red line) and centered training point (blue line).

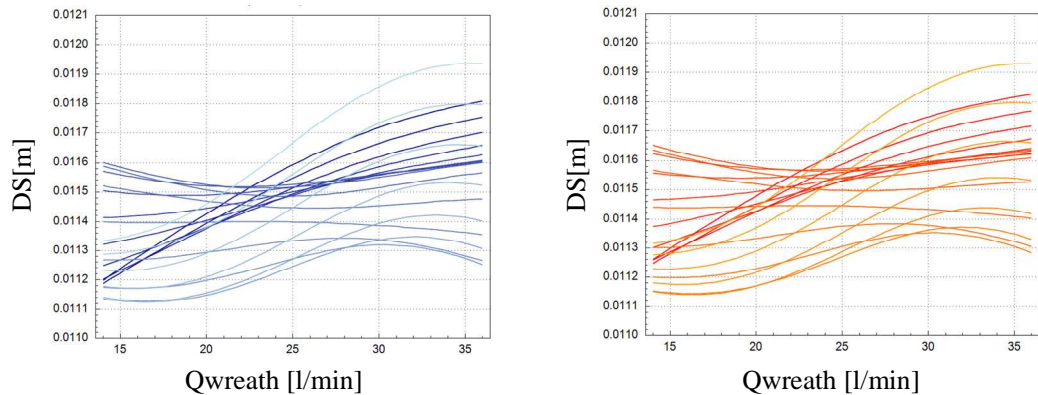


**Figure 105:** Shell thickness at the end of the mould as a function of the cooling flow rate in wreath spray system, calculated by the ANN model on centered verification point (red line) and centered training point (blue line).

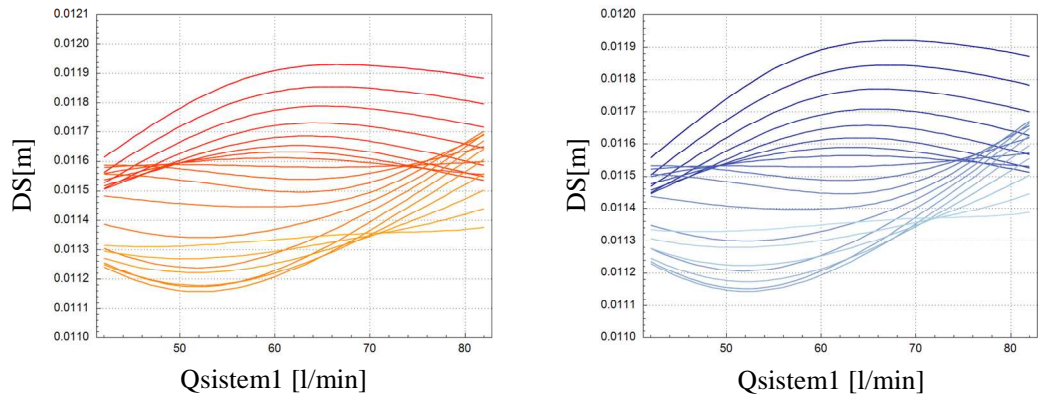


**Figure 106:** Shell thickness at the end of the mould as a function of the cooling flow rate in 1st spray system, calculated by the ANN model on centered verification point (red line) and centered training point (blue line).

#### 6.2.2.3 Billet Surface Temperature at Straightening Start Position (T)

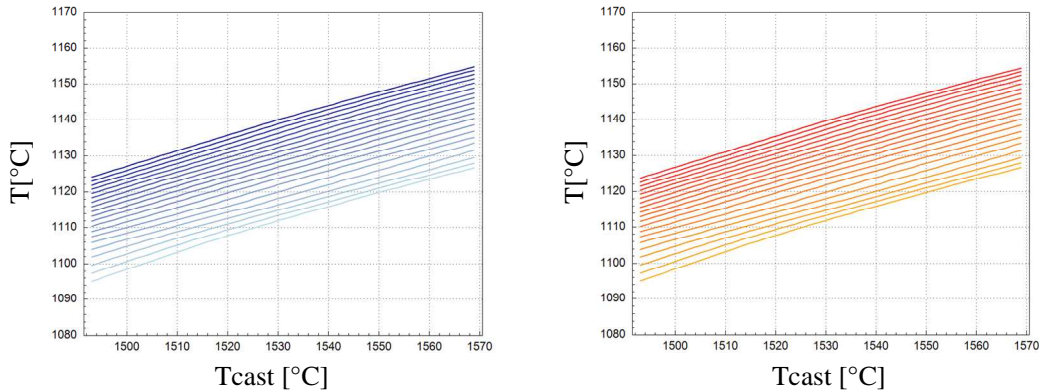


**Figure 107:** Billet surface temperature at straightening start position as a function of the casting temperature, calculated by the ANN model in two points from the data set, and for 18 other points on the line between them. Left: training data set. Right: verification data set.

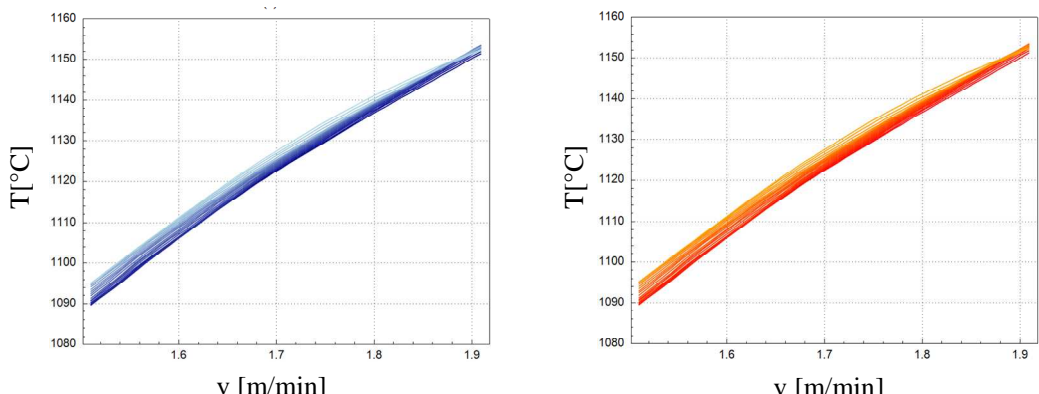


**Figure 108:** Billet surface temperature at straightening start position as a function of the casting speed, calculated by the ANN model on centered verification point (red line) and centered training point (blue line).

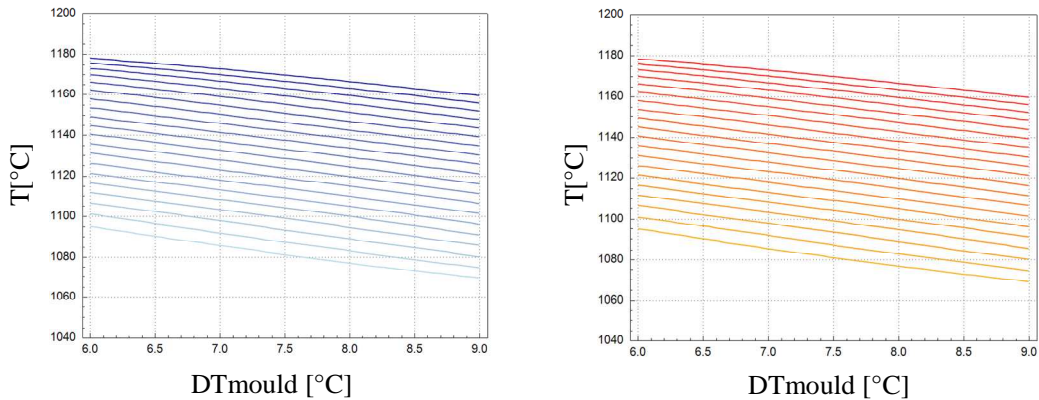


**Figure 109:** Billet surface temperature at straightening start position as a function of the temperature difference of cooling water in the mould, calculated by the ANN model on centered verification point (red line) and centered training point (blue line).

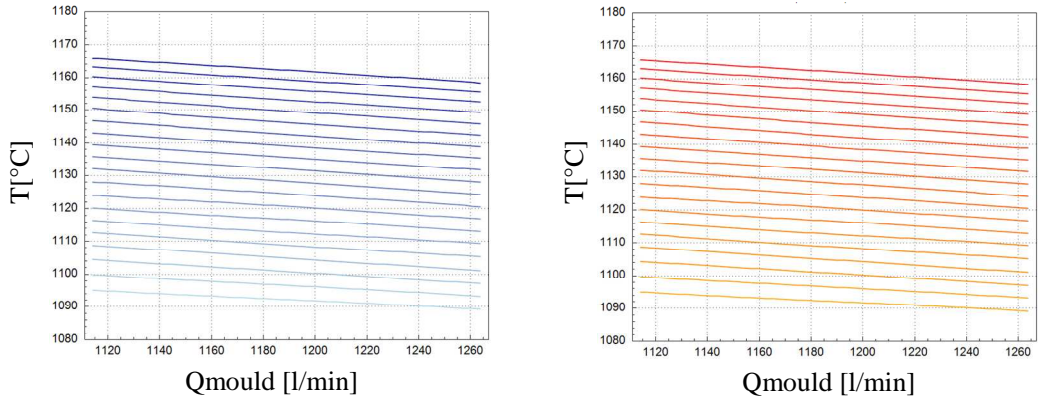


**Figure 110:** Billet surface temperature at straightening start position as a function of the cooling flow rate in the mould, calculated by the ANN model on centered verification point (red line) and centered training point (blue line).

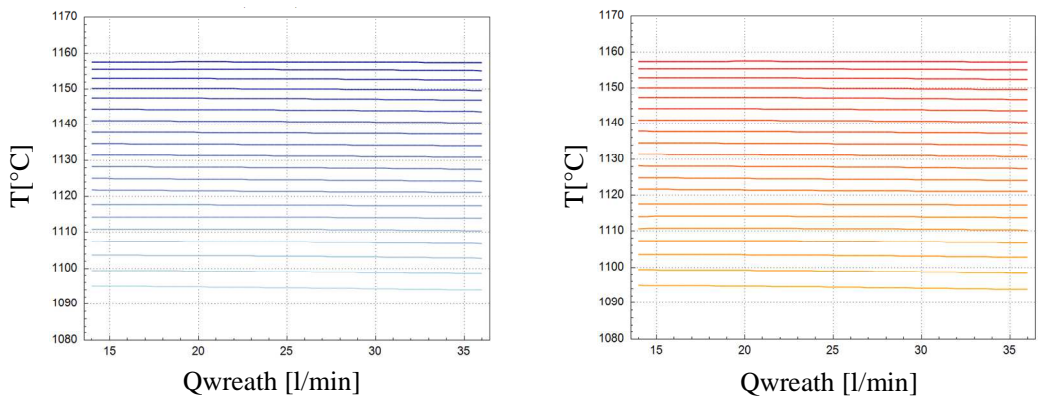


**Figure 111:** Billet surface temperature at straightening start position as a function of the cooling flow rate in wreath spray system, calculated by the ANN model on centered verification point (red line) and centered training point (blue line).

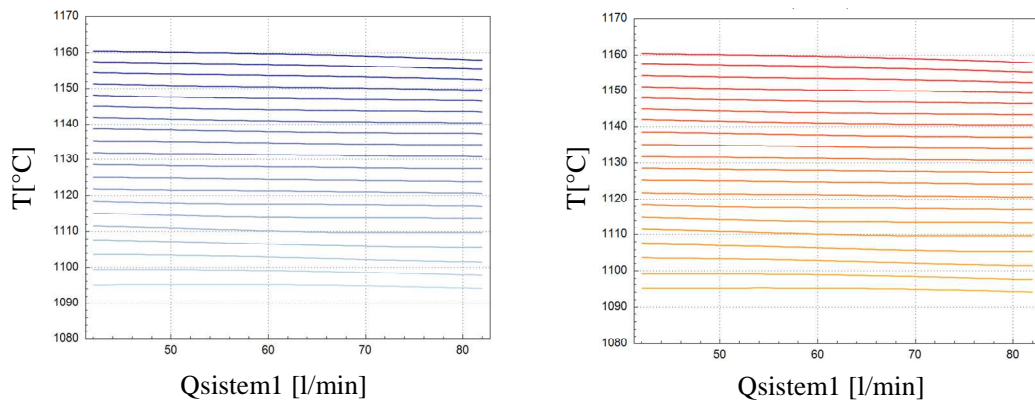


**Figure 112:** Billet surface temperature at straightening start position as a function of the cooling flow rate in 1st spray system, calculated by the ANN model on centered verification point (red line) and centered training point (blue line).

### 6.3 Sensitivity Tests

The main purpose of these tests is to demonstrate the influence of different process parameters on 3 outputs. In each test we change one process parameter from minimum value to maximum value and verify the change in all output values. The graph below shows how process parameters influence on outputs. The influence is represented in percentage of change of process parameter according to the range of that process parameter.

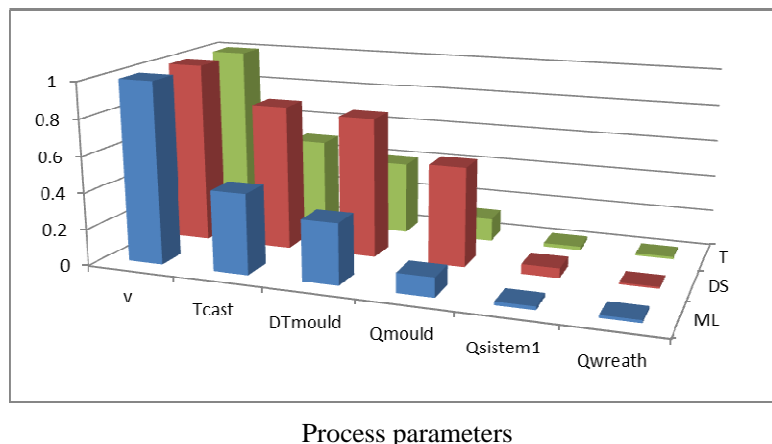


**Figure 113:** Influence on metallurgical length (ML), shell thickness at the end of the mould (DS) and billet surface temperature at straightening start position (T) by changing process parameters from minimum to maximum value.

#### 6.3.1 Metallurgical Length (ML)

Graph below shows the influence of different process parameters to metallurgical length (ML) for verification point. Process parameters are sorted from the most influential to the least influential. The influence is represented in value of change of process parameter on output quantity (ML).

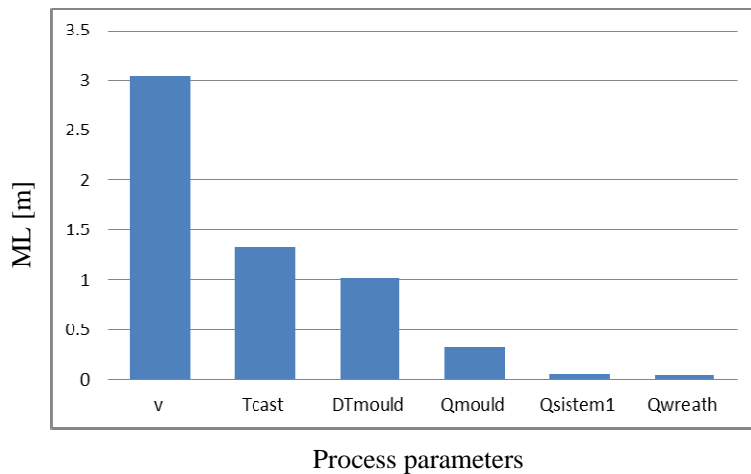


**Figure 114:** Influence on metallurgical length (ML) by changing process parameters from minimum to maximum value for verification point. Influence is shown in value of total range of metallurgical length (ML).

Influence of each process parameter on output is different. In the Figure 115 we can see the share of each process parameter in percentage among all process parameters when simulating metallurgical length (ML).

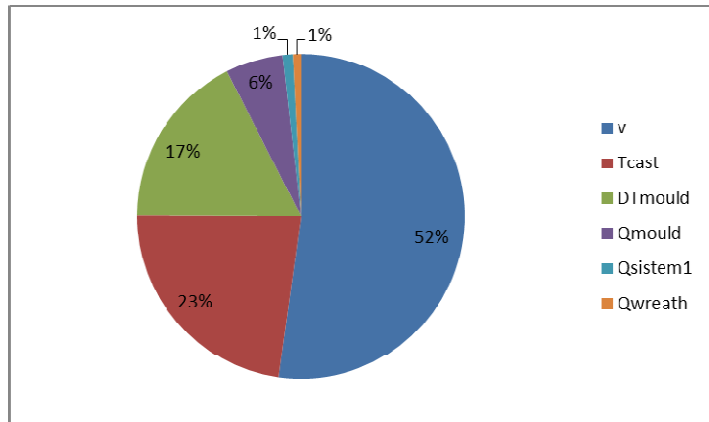


**Figure 115:** The share of each process parameter in percentage among all process parameters when simulating metallurgical length (ML).

### 6.3.2 Shell Thickness at the End of the Mould (DS)

Graph below shows the influence of different process parameters to metallurgical length (DS) for verification point. Process parameters are sorted from the most influential to the least influential. The influence is represented in value of change of process parameter on output quantity (DS).

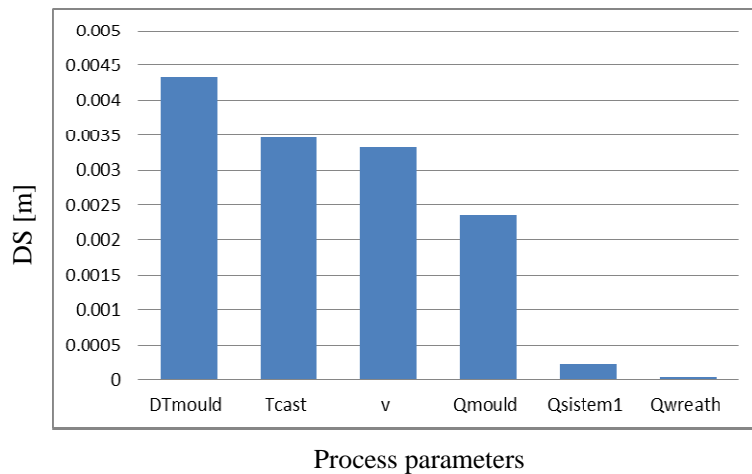


**Figure 116:** Influence on shell thickness at the end of the mould (DS) by changing process parameters from minimum to maximum value for verification point. Influence is shown in value of total range of shell thickness at the end of the mould (DS).

Influence of each process parameter on output is different. In the Figure 117 we can see the share of each process parameter in percentage among all process parameters when simulating shell thickness at the end of the mould (DS).

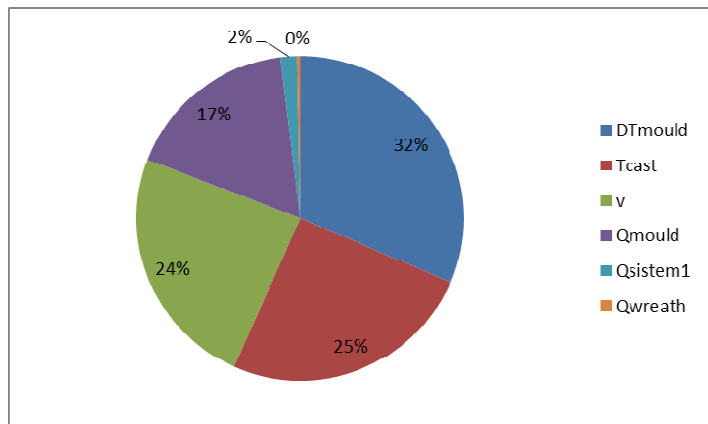


**Figure 117:** The share of each process parameter in percentage among all process parameters when simulating shell thickness at the end of the mould (DS).

### 6.3.3 Billet Surface Temperature at Straightening Start Position (T)

Graph below shows the influence of different process parameters to metallurgical length (T) for verification point. Process parameters are sorted from the most influential to the least influential. The influence is represented in value of change of process parameter on output quantity (T).

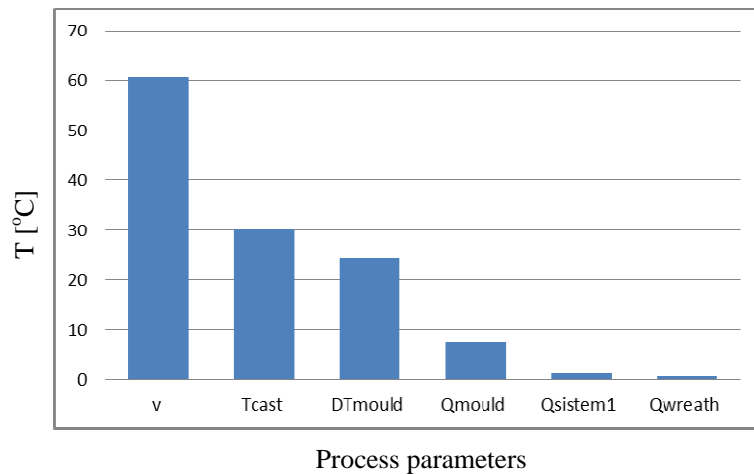


**Figure 118:** Influence on billet surface temperature at straightening start position ( $T$ ) by changing process parameters from minimum to maximum value for verification point. Influence is shown in value of total range of billet surface temperature at straightening start position ( $T$ ).

Influence of each process parameter on output is different. In the Figure 119 we can see the share of each process parameter in percentage among all process parameters when simulating billet surface temperature at straightening start position ( $T$ ).

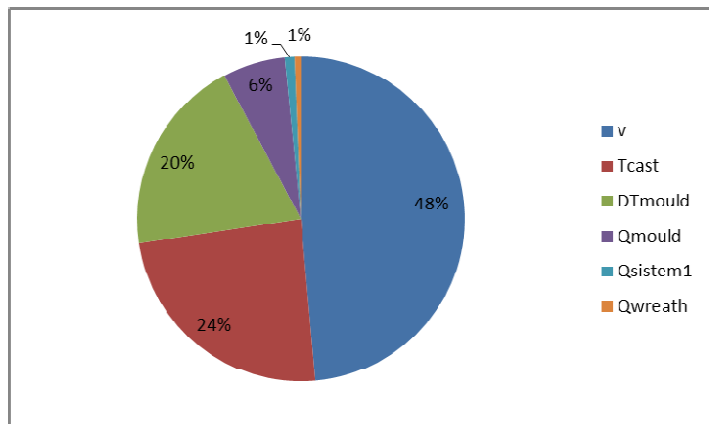


**Figure 119:** The share of each process parameter in percentage among all process parameters when simulating billet surface temperature at straightening start position ( $T$ ).

### References:

- [1] Store Steel d.d. (2012). Available at: <http://www.store-steel.si/ProizvodniProgramE.asp>.
- [2] Vertnik, R. (2006) Local collocation method for phase-change problems. Ms.C. thesis, University of Nova Gorica, Slovenia.
- [3] Vertnik, R. (2010). Heat and fluid flow simulation of the continuous casting of steel by a meshless method. PhD Thesis. University of Nova Gorica, Slovenia.
- [4] Vertnik, R. and Šarler, B. (2009). Simulation of continuous casting of steel by a meshless technique. International Journal of Cast Metals Research, vol. 22, pp.311-313.
- [5] Grešovnik, I.; Kodelja, T.; Vertnik, R.; Šarler, B. (2012): Application of artificial neural networks to improve steel production process. Bruzzone, A. G.; Hamza, M. H. Proceedings of the 15th International Conference on Artificial Intelligence and Soft Computing, Napoli, Italy, pp. 249-255.
- [6] Grešovnik, I.; Kodelja, T.; Vertnik, R.; Senčič, B.; Kovačič, M.; Šarler, B. (2012): Application of artificial neural networks in design of steel production path. Computers, Materials and Continua, vol. 30, pp. 19-38.
- [7] Kodelja, T.; Grešovnik, I.; Vertnik, R.; Šarler, B. (2012): Topmost steel production design by using artificial neural networks through process modeling, 20<sup>th</sup> jubilee conference on materials and technology, Portorož, Slovenia.
- [8] Gresovnik, I. (2000): A General Purpose Computational Shell for Solving Inverse and Optimisation Problems - Applications to Metal Forming Processes, Ph. D. thesis, University of Wales Swansea, U.K..
- [9] Grešovnik, I. (2012): Optimization shell Inverse, <http://www2.arnes.si/~ljc3m2/inverse/>.
- [10] Grešovnik, I. (2007): The use of moving least squares for a smooth approximation of sampled data. Journal of Mechanical Engineering, vol. 9, pp. 582-598.
- [11] Grešovnik, I. (2009): Simplex Algorithms for Nonlinear Constrained Optimization Problems, technical report. Available at:  
<http://www2.arnes.si/~ljc3m2/igor/doc/rep/optalgsimplex.pdf>.
- [12] Grešovnik, I. (2012): IOptLib – library for solving inverse and optimization problems. Available at: <http://www2.arnes.si/~ljc3m2/igor/ioplib/> .
- [13] Grešovnik, I. (2012): IGLib.net - investigative generic library. Available at:  
<http://www2.arnes.si/~ljc3m2/igor/iglib/>.
- [14] Aforge.Net, artificial intelligence library (2012). Available at:  
<http://www.aforgenet.com/>.
- [15] Grešovnik, I.; Kodelja, T.; Vertnik, R.; Šarler, B. (2012): A software framework for optimization parameters in material production. Applied Mechanics and Materials, vol. 101, pp. 838-841.

## **References**

---

- [16] Grešovnik, I.; Kodelja, T.; Vertnik, R.; Šarler, B. (2012): A software Framework for Optimization Parameters in Material Production. *Applied Mechanics and Materials*, vol. 101-102, pp. 838-841. Trans Tech Publications, Switzerland.
- [17] Grešovnik, I.; Kodelja, T.; Vertnik, R.; Šarler, B. (2012): Application of artificial neural networks to improve steel production process. Bruzzone, A. G.; Hamza, M. H. Proceedings of the 15th International Conference on Artificial Intelligence and Soft Computing, Napoli, Italy, pp. 249-255.